Physics – Uspekhi **50** (2) 115 – 139 (2007)

REVIEWS OF TOPICAL PROBLEMS PACS numbers: **95.75.–z**, 98.52.Nr, 98.62.Hr

Prediction and discovery of new structures in spiral galaxies

A M Fridman

DOI: 10.1070/PU2007v050n02ABEH006210

Contents

Abstract. **A review is given of the last 20 years of published research into the nature, origin mechanisms, and observed features of spiral-vortex structures found in galaxies. The so-called rotating shallow water experiments are briefly discussed, carried out with a facility designed by the present author and built at the Russian Scientific Center 'Kurchatov Institute' to model the origin of galactic spiral structures. The discovery of new vortex-anticyclone structures in these experiments stimulated searching for them astronomically using the RAS Special Astrophysical Observatory's 6-meter BTA optical telescope, formerly the world's and now Europe's largest. Seven years after the pioneering experiments, Afanasyev and the present author discovered the predicted giant anticyclones in the galaxy Mrk 1040 by using BTA. Somewhat later, the theoretical prediction of giant cyclones in spiral galaxies was made, also to be verified by BTA afterwards. To use the observed line-of-sight velocity field for reconstructing the 3D velocity vector distribution in a galactic disk, a method for solving a problem from the class of ill-posed astrophysical problems was developed by the present author and colleagues. In addition to the vortex structure, other new features were discovered — in particular, slow bars (another theoretical prediction), for whose discovery an observational test capable of distinguishing them from their earlier-studied normal (fast) counterparts was designed.**

A M Fridman Institute of Astronomy, Russian Academy of Sciences, ul. Pyatnitskaya 48, 119017 Moscow, Russian Federation
Tel. (7-495) 951 79 93. Fax (7-495) 230 20 81
E-mail: afridman@inasan.rssi.ru
Russian Research Center 'Kurchatov Institute', Institute of Physics of Stochastic Structures, pl. Kurchatova 1, 123182 Moscow, Russian Federation

Received 7 September 2006, revised 2 October 2006
Uspekhi Fizicheskikh Nauk **177** (2) 121 – 148 (2007)
Translated by K A Postnov; edited by A M Semikhatov

1. Introduction

Astrophysical studies of the last few decades have demonstrated that most evolutionary processes in the metagalaxy are related to collective effects. Different instabilities that develop on all scales of hierarchical structures in the universe are the main driving force of evolution. The queen of instabilities — the gravitational instability — created the entire observed hierarchy of structures, from stars and star clusters up to galaxies and galaxy clusters. On each scale, specific instabilities operate and form structures specific to this scale.

Astrophysical disks, and especially disks in spiral galaxies, represent unique natural test beds where most of the known instabilities in the metagalaxy develop. These instabilities then lead to the formation of regular structures, stationary convective flows, turbulence, and chaos.

The richness of structures observed in disks of spiral galaxies follows from numerous collective processes, both linear and nonlinear, that have been developing in the disks. Most of them can also be found (usually less pronounced) in other astronomical phenomena of different sizes, but just spiral galaxies can be considered natural laboratories for studying collective processes. Some of these instabilities are also investigated in physics, mechanics, and mathematics. That is why we believe that theoretical and observational discoveries of recent years, which we wish to describe in the present review, are important and interesting for a broad community of astronomers, physicists, mechanicians, and mathematicians.

The work "Prediction and discovery of new structures in spiral galaxies," which was awarded the State Prize in 2003, includes a collection of papers started more than 30 years ago (in 1972) and carried out under the leadership of the present author. The group included observers, interpreters of astronomical data, theorists, and experimentalists investigating one scientific problem.

This group predicted and discovered new structures — giant vortices (cyclones and anticyclones) and slow bars in spiral galaxies. Spiral vortices were observed in the two-dimensional velocity field of gaseous disks in spiral galaxies. To prove the existence of slow bars, the rotation curve of gaseous disks taking the gas motion in large-scale vortices into account had to be constructed. Therefore, to discover these galactic structures, measurements and analysis of the line-of-sight velocity field of gas in the plane of galactic disks were required.

Before the work on this problem was started, the velocity field of galaxies had been measured with the 6 m BTA (Big Telescope Azimuthal) telescope of the Special Astrophysical Observatory (SAO) of the Russian Academy of Sciences (RAS) with the use of a long-slit spectrograph. The adding of measurements performed with different slit orientations led to errors too large to attain the accuracy needed to estimate systematic deviations of gas velocities from expected circular motions in a galaxy.

SAO RAN in collaboration with Observatoire de Marseille (France) designed and manufactured the set of devices, including a Fabry – Perot interferometer, for precise measurements of velocity fields in galaxies using the Doppler shifts of emission lines with the accuracy better than 10 km s^{-1}. Such a device was made in Russia for the first time. The discovery of new galactic structures was made possible only using this instrument.

The present review gives some details of the prediction and discovery of new structures in spiral galaxies, describes some scientific problems that had to be solved in pursuing these purposes, and outlines prospects in our understanding of the physics of galaxies.

In the present review we tried to avoid using special terminology and complicated mathematics. A more rigorous description can be found in the original papers cited in the references.

2. Experimental modeling of the galactic spiral structure generation and the prediction of giant anticyclones

Vortices between spirals, strikingly similar to spiral arms in galaxies, were first discovered in a laboratory setup with rotating 'shallow water,' which was specially designed by Snezhkin at the Russian Scientific Center 'Kurchatov Institute' to model the process of generating galactic spiral arms; it was thereafter called the 'Spiral' (Fig. 1a, b). The first version of this setup has a cone-like central unit with an almost flat periphery; in the second modification, both parts have a parabolic form. The bottom makes the liquid rotate, with a rotation velocity jump created between the central part and the periphery at some radius R with the width close to the liquid depth H_0. As a result, a jump in the radial profile of the rotation velocity emerges in the shallow water layer (Fig. 1c), imitating the jump in the rotation curve of a galaxy; due to hydrodynamic instability, this jump is capable of generating spiral density waves. This allowed using the Spiral setup to model dynamic processes in gaseous disks of galaxies with rotation velocity jumps.

The aim of the experiment was to check the possible generation of spiral density waves by a gravitohydrodynamic instability, which can be related to rapid local drops (jumps) in gas rotation velocity, which is frequently observed in many real galaxies. These features were well noticed in rotation curves of galaxies obtained earlier by BTA [1]. A strong velocity jump is shown schematically in Fig. 1d. Observations suggested (taking the angular resolution of the telescope into account) that approximately half the spiral galaxies demonstrated at least 10 – 15% relative velocity jumps $\Delta v/v$ in their rotation curves. However, numerical simulations by Baev and

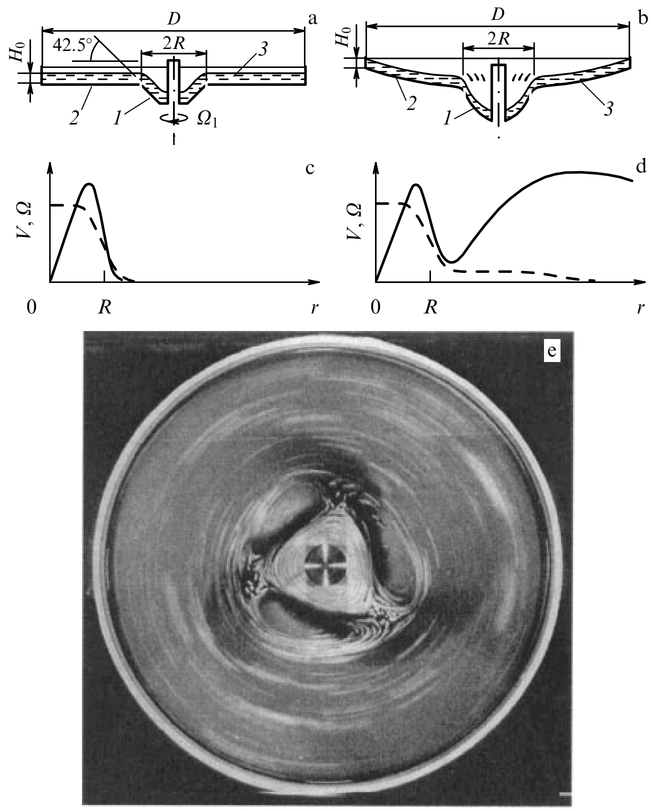

Figure 1. First (a) and second (b) modifications of the 'Spiral' setup: *1* — the central part rotating with angular velocity Ω_1, *2* — the outer part rotating with angular velocity Ω_2, *3* — the shallow water layer. In Fig. a: $D = 30$ cm, $R = 4$ cm; in Fig. b: $D = 60$ cm, $R = 8$ cm. Schematic radial profiles with a large rotation velocity jump of the shallow water (c) and gaseous galactic disk (d): solid and dashed lines correspond to the linear and angular rotation velocities, respectively. Anticyclones (e) between spiral density waves on the shallow water of the Spiral setup: three anticyclones correspond to three spiral arms.

Fridman [2] indicated that hydrodynamic effects are as important as gravitational ones in the mechanism of spiral arm formation in the gaseous disks of galaxies.

This point of view on the nature of spiral arms emerging in galaxies was put forward by the author in 1972 (see [3] and the references therein) and differed from the purely 'gravitational' theory of the generation of spiral arms that considers only self-gravitation forces [4]. The gravitational theory neglected the observed (sometimes very significant!) gradients of the main parameters of the disk.

First of all, using the Spiral setup, we checked the basic statements of the gravitohydrodynamic theory of spiral structure, which predicts a relation of the relative rotational velocity jump $\Delta v/v$ and the relative size of its spatial localization $\Delta R/R$ to the number of arms being generated. For this, a velocity jump imitating the features observed in rotation curves of galaxies was created using this setup (Fig. 1c). The rotating shallow water in the setup was described by equations of two-dimensional hydrodynamics [5]. This ensured the dynamical similarity of the rotating shallow water with gaseous disks of spiral galaxies and served as the starting point of further modeling. (Strictly speaking, it is the identity of the dynamical equations for self-gravitating gaseous disks and rotating shallow water that provided the theoretical basis for modeling [6, 7]).

The results of model experiments in shallow water [8] both confirmed the correctness of the gravitohydrodynamic theory of spiral structure formation and led to unexpected and original solutions of some problems related to certain features of the spiral structure such as the arm branching and the appearance of rarely observed 'leading' spirals. Moreover, they also showed something new: anticyclonic vortices were discovered between spiral arms in shallow water [9] (Fig. 1e). Hence, such vortices should be observed in real galaxies! Why then have they not been discovered over the long period of studies of the spiral structure, i.e., over more than one and a half centuries? We try to answer this question by looking at the history of studies of spiral galaxies.

2.1 Problem of the spiral structure of galaxies

In 1845, Lord Rosse in his family estate Birr Castle in Ireland designed and manufactured a 183 cm reflector with a focal length of 17 m, which was for a long time the world's largest instrument. This allowed him for the first time to discover the spiral structure in many nebulae, which for the subsequent seventy years were thought to reside in our galaxy. Only in 1924 did Edwin Hubble, using the telescope at the Mount Wilson Observatory (USA), which was the largest at that time with the primary mirror diameter 2.5 m, firmly establish that nebulae like those where Rosse discovered a spiral structure are in fact individual spiral galaxies.

Approximately at the same time, in the famous book *Astronomy and Cosmology* [10], Jeans wrote that in his opinion, "in spiral nebulae totally unknown forces operate" and only they can explain "the failure of attempts to understand the origin of spiral arms." The main difficulty here was that galaxy disks, in whose planes spiral arms are located, rotate differentially: the angular rotation velocity decreases inversely proportional to the distance from the galaxy center in the main part of the disk. This implies that if spiral arms, which are concentrations of gas and young stars, rotate differentially in the same way as the gaseous disk where they are observed, they must stretch after 1 – 2 turns of the periphery such that it would be difficult to distinguish them against the background. But our spiral galaxy in the solar vicinity has made around 50 turns keeping a distinct spiral structure.

In 1938, Bertil Lindblad managed to resolve this paradox. He proposed that spiral arms are density waves. The wave front rotates with a constant angular velocity by definition. Therefore, no 'stretching' of the wave occurs in a differentially rotating disk.

The wave theory of spiral structure was later rediscovered by Lin and Shu, who with co-authors essentially developed this theory and posed several principal questions to the observers. The main issue was to determine the angular rotation velocity of the spiral pattern. In the gravitational approach, this value cannot be found, it is a free parameter to be taken from observations. Its determination is equivalent to finding the radius of the corotation circle, where the constant angular velocity of spirals coincides with that of the differentially rotating galactic disk. Only recently our group published papers describing a canonical method for determining this principal parameter in spiral galaxies [11, 12]. In Section 4, we briefly describe the method that enabled us to solve one of the main problems: — finding the predicted anticyclones in gaseous disks of spiral galaxies. But we begin with an attempt to explain the essence of a generalization of the purely gravitational concept of the formation of spiral arms.

2.2 Gravitohydrodynamic concept of the generation of spiral arms

The gravitohydrodynamic concept [3, 6, 13], which includes the pure gravitational concept as a particular case, accounts for the self-gravitation force and gradients of the main unperturbed parameters, the density and rotation velocity, which are neglected in the purely gravitational concept. Figures 2a, b show radial profiles of the linear rotation velocity and the surface density in our Galaxy. The relative rotation velocity jump in central parts of the gaseous disk (at distances from 0.4 kpc to 1.2 kpc from the center) is $\approx 40\%$, while the jump in the gas surface density in the region of the maximum velocity gradient (at the distance ≈ 0.7 kpc from the center) attains almost two orders of magnitude. How is it possible to ignore such gradients in this case, where the hydrodynamic instability turns out to be much stronger than the gravitational one?

Our group investigated rotation curves (i.e., radial dependences of the rotation velocity) of spiral galaxies using the 6 m telescope [1]. As noted above, velocity jumps exceeding 10 – 15% are observed in almost half the cases of an arbitrary sample of spiral galaxies. Figure 2c shows rotation profiles of some galaxies. These velocity jumps can give rise to a centrifugal instability [6, 8, 9, 13] generating spiral density waves — the galactic spiral arms.

The centrifugal instability belongs to the class of shear flow instabilities. The necessary condition for a large-scale perturbation to grow is typically given by $kL \lesssim 1$, where k is the wave vector of the perturbation along the velocity jump and L is the width of 'smearing' of the shear flow. At $k \equiv 2\pi/\lambda$, where λ is the perturbation wavelength, the instability condition implies that the shear flow width L is small compared to the wavelength. The instability results in 'smearing' the value L until the stability boundary is reached, where only waves satisfying the condition

$$k_\varphi L \simeq 1 \tag{1}$$

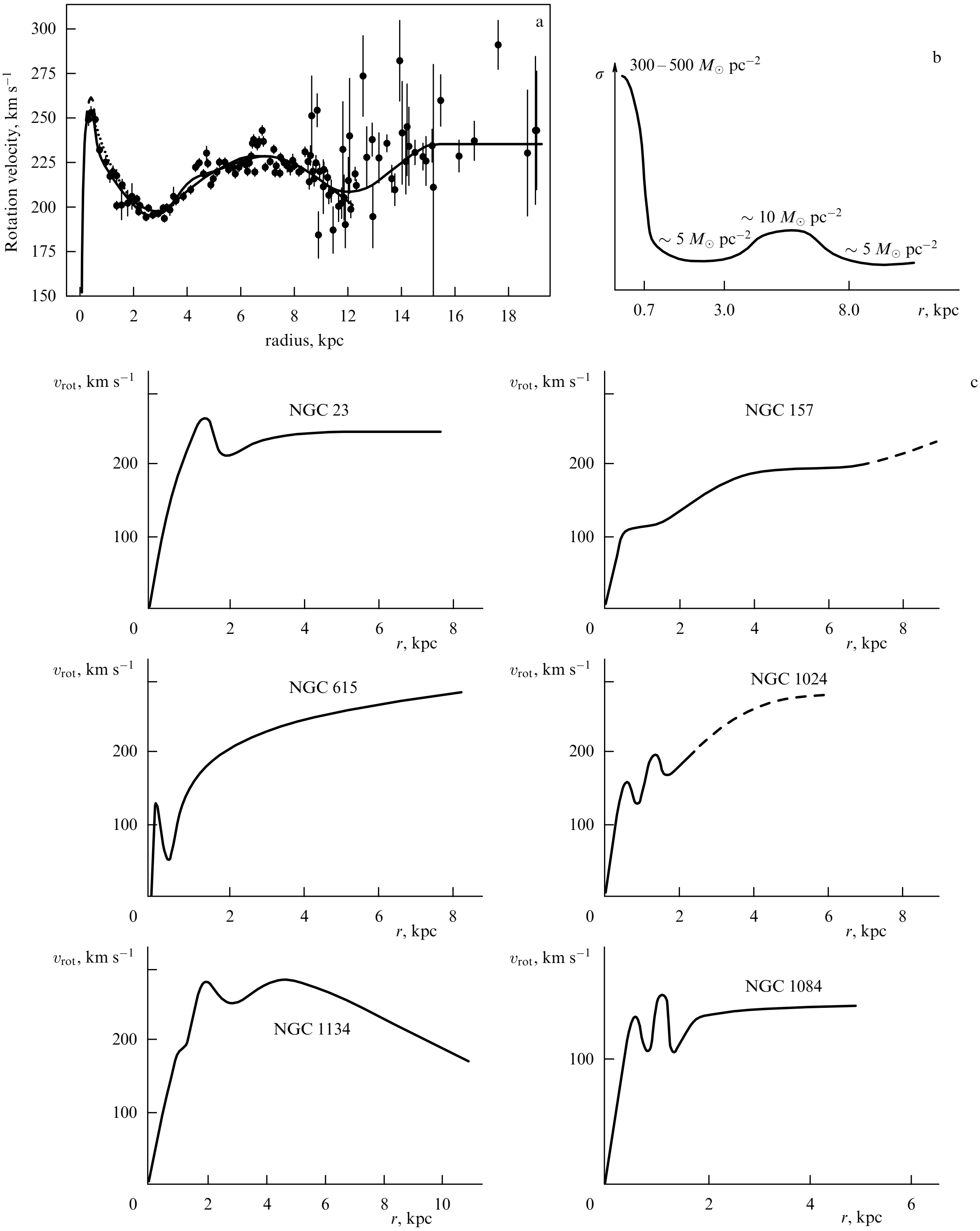

Figure 2. (a) The observed rotation velocity profile of our Galaxy with two velocity jumps [14]: one of them (the larger) is located near the center, the maximum of its negative velocity derivative lies at 0.7 kpc; the other (more distant) is located in the solar vicinity. (b) The gas density profile in the disk of our Galaxy; 1.989×10^{30} kg is the solar mass. (c) The rotation curves of different galaxies with rotation velocity jumps obtained in early observations with BTA.

can persist. Here, k_φ is the azimuthal wavenumber (in a galaxy disk, the coordinate along the velocity jump is the azimuthal angle φ). By definition,

$$k_\varphi \equiv \frac{m}{R}, \tag{2}$$

where m is the number of galactic arms and R is the radius where the velocity jump occurs.

If now we introduce the parameter $q \equiv \Omega_2/\Omega_1$, where Ω_1 and Ω_2 are the respective rotation velocities of the center and periphery of the galaxy (before and after the velocity jump correspondingly), then, clearly, the higher the rotation velocity jump (i.e., the smaller the parameter q), the larger the value of the 'smearing' L. Qualitatively, this dependence can be represented in the form

$$L \simeq Aq^{-\alpha}, \quad \alpha > 0, \tag{3}$$

where A is a constant.

Substituting (2) and (3) in (1), we obtain the qualitative dependence between the number of arms and the dimensionless velocity jump q:

$$m \simeq \frac{R}{A} q^{\alpha}, \quad \alpha > 0. \tag{4}$$

Formula (4) implies that the larger the velocity jump in a galaxy (i.e., the smaller the value q), the smaller the number of its spiral arms.

In the gravitohydrodynamic theory, the exact formula relating m and q was obtained. Its correctness was tested for both spiral galaxies with known rotation curves and rotating shallow-water experiments. However, before describing the experiment, we must check its 'model' applicability for generating galactic spiral arms in the framework of the gravitohydrodynamic concept. The question formulated in the title of Section 2.3 then naturally arises.

2.3 What do the Spiral setup and gaseous disk of a galaxy have in common?

With the reference to the outstanding textbook *Hydrodynamics* [5] by Landau and Lifshits, we already pointed out one property shared by shallow water and the gaseous disk of a galaxy. However, there are two principal differences as well.

The first is that the Spiral setup has a bottom, owing to which shallow water has a near-bottom viscosity characterized by the Ekman number. Clearly, nothing similar exists in a gaseous disk of a galaxy. On the other hand, self-gravitation forces operate in the galaxy disk, which are absent in the shallow water in the Spiral setup.

As shown in [6], both these 'principal' differences are illusory. First, the Ekman number in the Spiral setup is small, i.e., the near-bottom viscosity is small. But most important seems to be the fact that the viscous decay time of perturbations in the shallow water of the Spiral setup is much longer than the growth time of the centrifugal instability. In other words, the near-bottom viscosity has no effect on generating (due to the instability) spiral density waves in shallow water. On the other hand, in the absence of the near-bottom viscosity, we would be unable to reproduce the required rotation velocity profile with a jump in such an easy way. In spiral galaxies, the rotation velocity profile in a gaseous disk is produced by the gravitational potential, mainly due to much more massive stellar subsystems (see, e.g., [15]). In this sense, stellar subsystems play the same role in producing the rotation curve of the gaseous disk as the bottom in the Spiral setup does. As regards the role of viscosity of the gaseous disk in generating spiral arms of real galaxies, it is insignificant for either developing the centrifugal instability caused by the velocity gradient or the gravitational instability in the absence of significant velocity gradients. In the absence of the above instabilities, viscosity can lead to the formation of some structures similar to those observed, e.g., in planetary rings [14]. However, no large-scale spiral arms are known to be generated due to viscosity.

We now turn to the second 'fundamental' difference between shallow water and gaseous galaxy disks due to self-gravitation forces of the latter. In [6], a new quantity was introduced into the system of the initial dynamic equations for a self-gravitating disk, the speed of sound in a self-gravitating medium. This speed is smaller than that in a non-self-gravitating medium, because compression properties of a gas (the ability of a gas element to expand in response to the initial contraction) weaken in a self-gravitating medium: the compressed element is maintained by gravitational forces. If we substitute the speed of sound in a self-gravitating gas for the characteristic speed of wave propagation in shallow water, the equations for the galaxy disk transform into those for shallow water.

The above considerations suggest that the Spiral setup with rotating shallow water can indeed be used for laboratory modeling of the spiral structure generation in gaseous galaxy disks by hydrodynamic instability arising due to the rotation velocity gradient.

2.4 Hydrodynamic instabilities caused by a velocity jump

In Fig. 3, we show perturbations of the vortex sheet $\mathbf{v}$ along the x axis in two opposite limit cases, where the Mach number $M \equiv v/c$ (where c is the speed of sound) is much smaller (Fig. 3a) or much larger (Fig. 3b) than unity. According to Landau [17], the perturbation amplitudes on both sides of the z axis from the vortex sheet plane $z = 0$ decrease exponentially, $\sim \exp(-z/z_0)$. It therefore suffices to consider the region $|z| < z_0$.

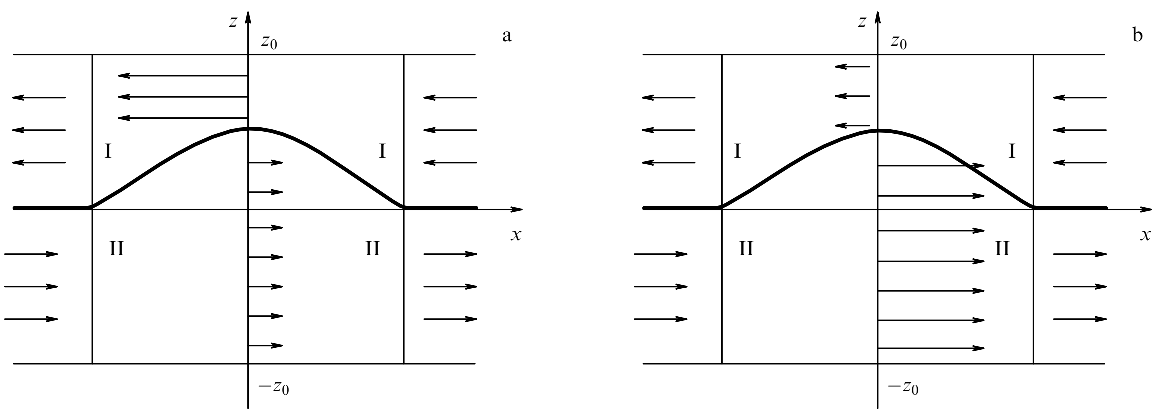

Figure 3. The schematic velocity distribution on both sides of the perturbed subsonic (a) and supersonic (b) vortex sheet.

Region I (above the perturbation 'bump') in Fig. 3a, b can be regarded as the region of motion inside a nozzle (more precisely, the longitudinal half of the nozzle). The character of motion in two nozzles, subsonic and supersonic, is radically different [18]. In the narrowest (critical) cross section of a subsonic nozzle, the velocity is maximum, as in the narrowest flow of a river. In the critical cross section of a supersonic diffuser, in contrast, the velocity is minimum. Hence, the different dynamics of two vortex sheets, subsonic and supersonic, are based on a constant value of the Bernoulli integral, $v^2/2 + W = \text{const}$, where W is the enthalpy. In the subsonic case, the velocity under the 'bump' is less than above the 'bump', $v_{\text{II}} < v_{\text{I}}$, and therefore $W_{\text{II}} > W_{\text{I}}$. Because the pressure usually increases with enthalpy, it follows that $P_{\text{II}} > P_{\text{I}}$, i.e., the 'bump' continues growing due to the pressure gradient. This is the physics behind the vortex sheet instability or (for a smoother velocity profile) of the Kelvin – Helmholtz instability.

In the supersonic velocity jump (Fig. 3b), we can write the opposite inequality $P_{\text{II}} < P_{\text{I}}$, i.e., the 'bump' is suppressed by the pressure gradient and no instability develops. The effect of stabilization of the supersonic vortex sheet was first noticed by Landau [17]. This effect occurs in the two-dimensional case, such as in a thin gaseous layer or shallow water. In a real three-dimensional medium, stabilization also occurs, but becomes effective only for large Mach numbers [19].

Velocity jumps observed in gaseous galaxy disks are supersonic (the typical value of the speed of sound or velocity dispersion of gas clouds in the interstellar gas is 10 km s^{-1}, whereas the rotation velocity of gaseous disks is ≈ 200 km s^{-1}). Therefore, the Landau stabilization criterion is satisfied for such disks: no vortex sheet instability or the Kelvin – Helmholtz instability develops there. However, another instability, a centrifugal one, is present. It can develop at arbitrarily large Mach numbers under the condition that the angular velocity of rotation of the central part (internal with respect to the velocity jump) is larger than that of the periphery: $q = \Omega_2/\Omega_1 < 1$. This condition is always satisfied for disks of spiral galaxies.

Thus, creating a velocity jump in shallow water exceeding the characteristic propagation velocity of perturbations is analogous to creating a supersonic velocity jump in the gaseous disk of a galaxy, which is actually observed in spiral galaxies [1]. We consider the results of this experiment immediately after giving a brief description of the experimental setup and the method of diagnostics of spiral density waves and the velocity field in shallow water.

2.5 Modeling spiral structure generation in galaxies using the Spiral setup

2.5.1 The Spiral setup and diagnostics. Both modifications of the Spiral setup have the same principal scheme: a cylindrical vessel consisting of two parts, the 'central' part and the 'periphery,' with the central part capable of spinning independently of the periphery. In the first modification, the central part has a conical shape and the periphery is almost flat (Fig. 1a). In the second modification (Fig. 1b), both parts consist of two paraboloids whose size is twice as large as in the first modification. The spinning bottom makes the liquid rotate such that at a radius R between the central part and the periphery, a rotation velocity jump emerges with the initial width close to the liquid depth H_0. As a result, a layer of the shallow water exhibits a jump on the radial profile of the rotation velocity (Fig. 1c). The diagnostics used in the Spiral setup allow determining the structure of both the density waves and the perturbation velocity field of the shallow water.

A white-bottom vessel is filled with a green liquid solution; in black-and-white photography made through a red filter, the density wave 'crests' look darker than the 'troughs' between them. The velocity field is determined using the direction and length of tracks (over the exposure time) left by 1 – 2 mm paper circles floating on the surface of the liquid. The camera rotates with an adjustable angular velocity coaxially with the Spiral rotation. Further details on the Spiral setup can be found in [20].

2.5.2 The relation between the number of arms and the velocity jump. The consistency of the hydrodynamic theory for spiral structure generation with the results of model experiments is demonstrated in Fig. 4a, which shows that the number of spiral arms increases with the parameter q, in accordance with formula (4).

2.5.3 Trailing and leading spirals. Different spiral patterns of galaxies are characterized not only by the number of arms but also by the shape of the spirals. First of all, 'trailing' and 'leading' spirals can be distinguished (Fig. 4b, c). The former

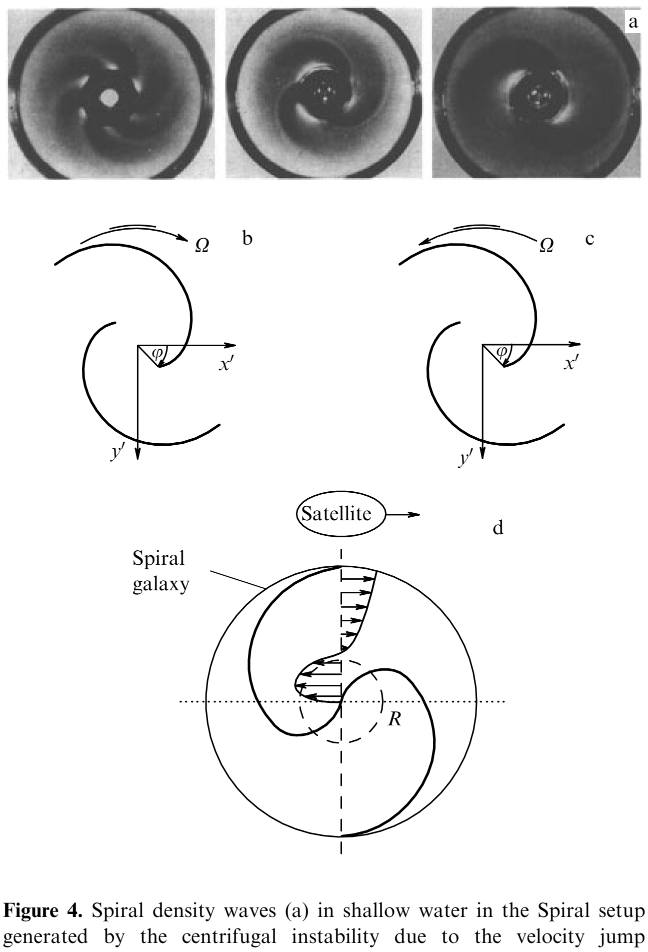

Figure 4. Spiral density waves (a) in shallow water in the Spiral setup generated by the centrifugal instability due to the velocity jump $q \equiv \Omega_2/\Omega_1 < 1$, where Ω_1 and Ω_2 are the respective angular rotation velocities of the central part and periphery; as the velocity jump decreases (the parameter q increases), the number of spiral arms increases [see Eqn (4)] (q decreases from left to right). Schematic plots of trailing (b) and leading (c) spirals (the arrow indicates the direction of galaxy disk rotation) and the possible excitation mechanism (d) of leading spirals.

rotate with backward-pointed ends and therefore have a good 'aerodynamic' form. The vast majority of spiral arms are trailing.

Using a random sample of 109 spiral galaxies, Pasha has shown that three of them have leading spiral arms [21]. Each of these three galaxies has a close satellite, but only for one of them was the direction of the orbital angular momentum of the satellite relative to the 'spin' axis of the galaxy measured: they turned out to be opposite.

When we changed the sign of the angular velocity of the periphery in the Spiral setup, i.e., replaced $\Omega_2 \to -\Omega_2$, we discovered leading spiral density waves. The author of the present review put forward the idea that in rarely observed galaxies with leading spiral arms, the role of the counter-rotating external disk can be played by a satellite perturbing the main galaxy disk, if it rotates in the galaxy plane in the opposite direction (Fig. 4d).

2.5.4 Branching of spirals. This phenomenon is so widespread that its absence can be considered an exception. The branching typically occurs 'outwards': by moving along an arm toward the periphery, we meet a region where the arm splits into two parts. Exactly the same picture is observed in the image of the spiral pattern in shallow water (Fig. 5a). We recall that different (but constant at the instant the image is taken) values of q correspond to different numbers of spiral arms. In contrast to the image shown in Fig. 1e, which was taken at a constant q, here the image was taken at the instant when the parameter q was decreasing. If the value of q was initially near the boundary of the instability of generating four-arm waves ($m = 4$), then two-arm waves ($m = 2$) are generated at the moment the image is taken. Wave generation occurs near the velocity jump, where the mode $m = 2$ is observed. The periphery, as usual, 'learns' that the center has already switched to another mode with a delay, and we therefore observe the old mode ($m = 4$) at the periphery. As a result, 'branching' occurs, which reflects the disk evolution: a velocity increase in its central part relative to the periphery or, inversely, a relative velocity decrease at the periphery. The first case is possible, for example, when the central part contracts, and the second case when the periphery expands.

2.6 Vortices between 'shallow water' spirals

The immobile camera fixed the trajectories of particles (stream lines), which are frequently encountered in astronomical papers devoted to the velocity fields in galaxies but give little information (Fig. 5b). The camera that rotated synchronously with the spiral arms, i.e., with the same angular velocity, detected anticyclones (Fig. 5c).

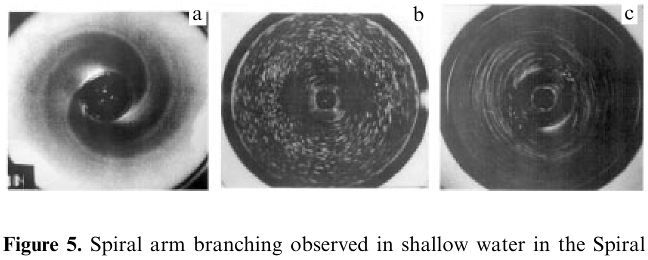

Figure 5. Spiral arm branching observed in shallow water in the Spiral setup as the velocity jump changes (a), and the stream lines in the case of generation of a two-arm density wave: (b) the camera is at rest relative to the rotating shallow water, (c) the camera rotates with the angular velocity of the spirals.

3. Discovery of giant anticyclones in galaxies with a sharp jump in the rotation velocity curve (example of the galaxy Mrk 1040)

The identity of the equations for shallow water and the gaseous disk of a galaxy [6], the quantitative agreement between experimental results showing the dependence of the number of spiral arms on the Mach number [8] at the velocity jump, and the experimental confirmation of the purely 'astronomical' hypotheses on the nature of arm branching and leading spirals — these facts are evidence that the rotating shallow water in the Spiral setup successfully models dynamic processes and structures in gaseous disks of spiral galaxies. Therefore, the appearance of anticyclones between spiral arms on the surface of shallow water with the size only two times smaller than the arm length left no doubt that similar vortices exist in spiral galaxies. The task was then to discover them in observations.

We ask the question: what conditions must the best candidate spiral galaxy satisfy to show such features?

As can be seen from experimental results, the centers of anticyclones are located at the velocity jump and structures — spirals and vortices — are caused by hydrodynamic instability. We therefore needed to find a galaxy with a large rotation velocity jump which, undoubtedly, would cause this instability.

But the candidate spiral galaxy should satisfy not only this condition. It must be 'properly oriented' in space relative to the observer (Fig. 6a). We now explain what this means.

The anticyclones we want to find in the frame corotating with spiral arms are characterized by closed stream lines in the galactic plane with centers at the corotation radius. At this radius, the disk rotation velocity relative to the spiral arms vanishes. But the perturbed velocity of gaseous clouds is nonzero by virtue of the same instability that formed spiral density waves and vortices.

If we could measure, for example, only the perturbed azimuthal velocity, then in the case of a two-arm galaxy, we would observe two hypothetical points symmetrically located on the corotation circle on both sides of the center with oppositely directed perturbed azimuthal velocities in the inner and outer neighborhood of each point. This feature can be used as an observational criterion for the presence of an anticyclone in a galaxy disk.

However, we measure only the velocity of clouds directed along the line of sight toward the telescope. Generally, in addition to the azimuthal velocity, the line-of-sight velocity includes two additional components of the cloud velocity: the radial velocity and the component along the z axis (directed along the rotation axis). On the other hand, if the orientation of the gaseous disk of a galaxy were such that the azimuthal perturbed velocities in the vicinity of the center of vortices were aligned with the line of sight and the radial and z-component of the velocity were perpendicular to it, the latter two components would not contribute to the line-of-sight velocity. We would measure the azimuthal velocity only. The z-component does not contribute if we observe the disk almost edge-on ($i = \pi/2$). Radial velocities near the centers of vortices do not contribute if they lie practically on the line of nodes (the large dynamical axis) of the galaxy (Fig. 6a).

Exactly these conditions relative to the terrestrial observer are satisfied by the galaxy Mrk 1040, which shows a large sharp jump in the rotation velocity.

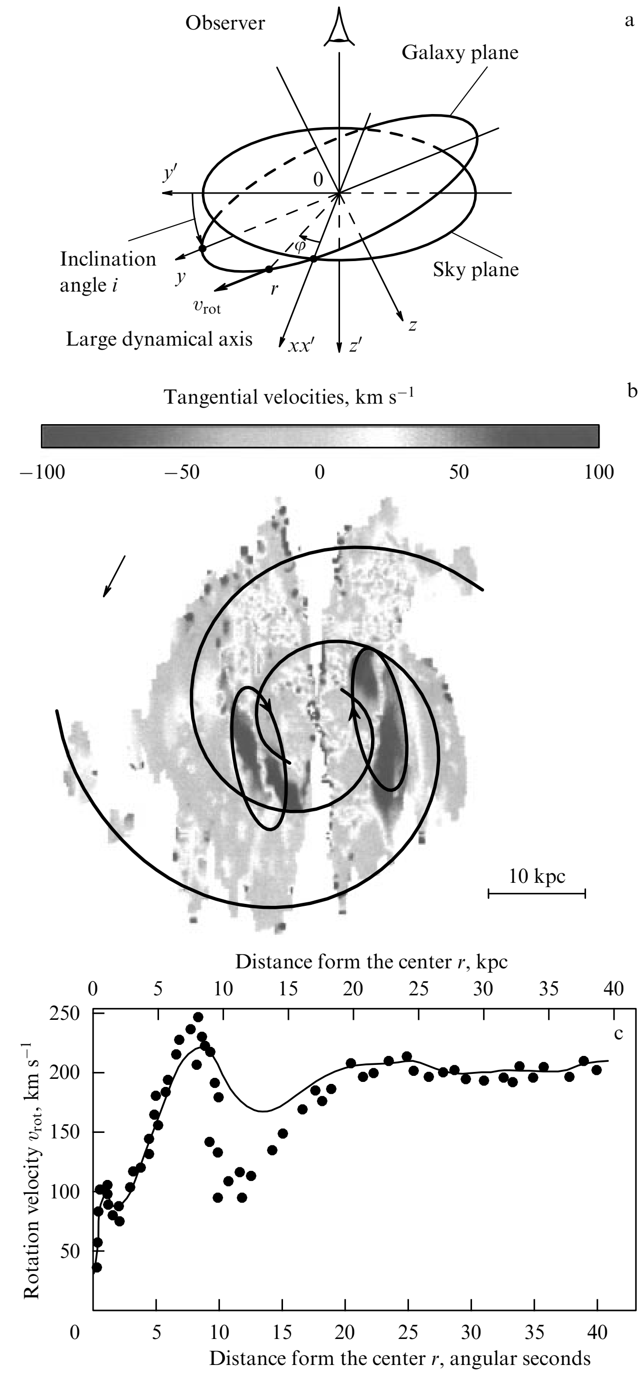

Figure 6. (a) Coordinates used to describe the position of a galaxy with respect to the observer and gaseous regions in the galaxy disk plane. The inclination angle i of the galaxy is the angle between the sky plane (perpendicular to the line of sight) and the galaxy plane; x' and y' are Cartesian coordinates in the sky plane; x and y are Cartesian coordinates in the galaxy plane; r and φ are polar coordinates in the galaxy plane, r is the galactocentric distance and φ is the galactocentric azimuthal angle counted from the 'line of nodes' — the crossing line of the galaxy with the sky plane. The line of sight is along the z' axis. (b) The map of tangential velocity $v_{\rm tang} \sim v_{\rm obs}/(\cos\varphi \sin i) - v_{\rm rot}$, $v_{\rm obs}$ is the observed velocity along the line of sight. The centers of anticyclones shown by ellipses with arrows are located fairly close to the line of nodes. (c) The comparison of the azimuthally averaged rotation curve with the velocity distribution along the line of nodes (filled circles) in the galaxy Mrk 1040.

Indeed, the inclination angle of the plane of this galaxy to the line of sight is $\sim 73°$, only $17°$ away from the edge-on view. As we can see from Fig. 6b, centers of anticyclones (which are shown by the looped curves with arrows) are located close to the line of nodes [22].

As can be seen in Fig. 6c, the radial velocity jump along the line of nodes (where vortices are localized) is enormous, more than 150 km s^{-1}, i.e., $\Delta v/v > 0.6$. The azimuthally averaged rotation velocity shows the jump $\Delta v/v \approx 0.3$. The radial velocity gradient is also anomalously high: $\mathrm{d}(\ln v)/\mathrm{d}(\ln r) \approx -3.1$, which corresponds to a very strong hydrodynamic instability [13].

4. Vortices in the solar vicinity

As noted above, the search for galactic anticyclones requires that the velocity field be found in the coordinate frame corotating with the spiral pattern. In the Spiral experiments, the rotation velocity of the spiral arms could be measured directly. But this is not so easy to do for real galaxies because the characteristic time of rotation in galaxy disks amounts to about a hundred million years, and it is therefore impossible to notice the rotation-induced shift of spiral arms over any reasonable time of observation.

The problem of measuring the spiral pattern rotation velocity is equivalent to finding the corotation radius, i.e., the radius where the galaxy disk rotates with the same velocity as the spirals. If the spiral wave is formed due to the instability induced by the velocity jump, its corotation radius coincides with the velocity jump location [6, 13]. In Mrk 1040, an anomalously sharp jump in the rotation curve is present and conditions for the hydrodynamic instability are satisfied, and hence the corotation radius in this galaxy can be readily determined. This has greatly facilitated the discovery of giant anticyclones in this galaxy [22]. Nevertheless, the problem of locating the corotation radius remains unsolved for most external galaxies.

It is thus not surprising that the next candidate where vortex structures should be sought was our Galaxy, in which the location of the corotation radius is best studied.

In this case, data on the so-called stellar age gradient has been used to determine the corotation radius. Star formation primarily occurs in spiral arms where enhanced concentration of young newborn stars is observed. Stars tend to move away from spiral arms with age. As the angular rotation velocity of the gaseous disk around the galactic center decreases with radius and the spiral pattern rotates as a whole with constant angular velocity, the region of the disk inside the corotation circle overtakes the spiral arms and the region outside it lags behind them. Stars have a 'memory' about the gaseous disk where they were formed. This implies that stars move faster than the spiral arms at distances from the galactic center inside the corotation radius, and move more slowly than the spiral arms beyond the corotation radius. As a result, the directions of stellar age gradients on both sides of the corotation circle must be opposite (Fig. 7, see the caption).

This feature of the age gradients was discovered in the solar vicinity [23, 24], which points to the location of the corotation circle near the sun (close to the solar orbit in the Galaxy). Studies of the line-of-sight velocity field of Cepheids in the solar neighborhood also suggested that in this region, the azimuthal velocity of the galactic spiral pattern coincides with the disk rotation velocity [25]. Thus, we see that different authors conclude that the sun resides near the corotation radius.

In addition, the observed rotation curve of the gaseous disk in our Galaxy exhibits a depression just near the solar

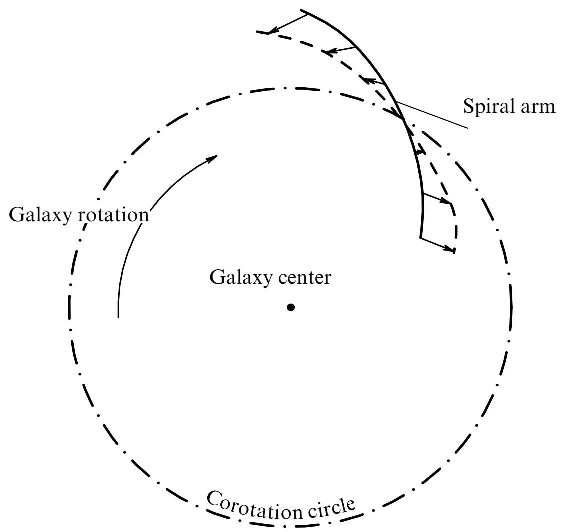

Figure 7. The gradient of stellar ages near the corotation circle. The region of an enhanced number density of young stars (shown by the solid line) coincides with the observed localization of the spiral arm. Older stars born in this arm have already shifted from this arm into the region shown by the dashed line. Their pathways are shown by small arrows whose length and direction are determined by the disk rotation velocity in the arm's reference frame; the long arrow indicates the galaxy rotation direction in the laboratory frame. Inside the corotation circle (dashed-dotted circle), the disk rotates faster than the spiral arm, and hence the direction of small arrows here coincides with the long arrow. Beyond the corotation circle, the direction of the small arrows is opposite. The stellar age gradient is directed along the small arrows, and therefore at the radius where it changes, its direction corresponds to the corotation radius (the dashed-dotted circle).

orbit. Based on these two facts, it was argued in [26] that there are centers of giant anticyclones in the vicinity of the galactic orbit of the sun.

This hypothesis was tested using data on the line-of-sight velocities of 316 molecular clouds, 256 classical Cepheids, and 106 young open clusters [11] (Fig. 8a).

Figure 8b demonstrates the rotation curve obtained in the model of purely circular motion [27]. More detailed studies have shown that deviations in velocities from purely circular motions are systematic and correlate with the observed spiral structures.

Figure 8c shows the model velocity field in the frame rotating with the angular velocity equal to the mean angular velocity of stars near the sun [11]. This velocity field has the form of an anticyclone with its center lying in the solar vicinity.

We note that in our Galaxy, the interstellar dust absorbing light makes it difficult to study the velocity field of stars. We can therefore investigate only a small part of the Galaxy and can barely see regions beyond the galactic center.

Observations of an external galaxy allow us to see the entire galaxy, which makes it possible to precisely determine its properties. It is in this direction that studies needed to be continued.

5. Spiral-vortex structure in galaxies

The discovery of predicted anticyclones in the gaseous disk of Mrk 1040 and in the solar vicinity was quite natural. In both cases, the observed rotation curve of the gaseous disk sharply decreases (has a depression) at some radius. This feature suggests either the presence of a jump in the real rotation curve, which can lead to hydrodynamic instability, or the presence of appreciable local deviations from circular motion. It is the first case that has been modeled in the Spiral experiments where vortex structures were first discovered.

However, as noted in Section 3, the Mrk 1040 galaxy demonstrates an anomalously large velocity jump in the presence of a nearby satellite. In the solar vicinity, the paucity of statistical data leads to significant errors and does not allow firmly establishing the actual discovery of an anticyclone. Therefore, the anticyclones discovered could be considered special structures that can be found only in peculiar galaxies with sharp rotation velocity jumps and are not a signature of any spiral galaxy with spiral density waves.

A qualitative consideration shows that this is not the case and that gaseous vortices are intrinsic features of spiral density waves irrespective of the nature of forces acting in the disk: hydrodynamic, self-gravitation, or tidal forces caused, for example, by a bar or a satellite of the galaxy (see [28] for a more rigorous mathematical proof of this fact).

We assume that some collective mechanism (instability) operating in the disk generates velocity and density perturbations. Insofar as perturbation amplitudes are small, their growth is described by the linear theory of instability. All perturbed values can then be easily expressed through one quantity, i.e., they are all proportional to each other. The perturbed velocity field of the disk, by transferring part of matter from one region to another, creates density enhancements in the form of spiral density arms in some regions and spiral density depressions in other regions.

A further increase in the amplitude of perturbed quantities results in a gas density increase in the spiral arms by several times, thus forming a nonlinear density wave that we observe as a spiral arm. But observations suggest that the values of the perturbed velocities in both disks, stellar and gaseous, are much smaller than the rotation velocity. The increase in the perturbation amplitude stabilizes the instability, and the spiral wave becomes quasi-stationary. Peculiarities of the velocity field caused by such a wave can be efficiently studied in a frame rotating with the angular velocity of spiral pattern Ω_{ph} (Fig. 8d). This rotating frame is convenient mostly because spiral arms are at rest there, i.e., the perturbed surface density and the perturbed velocity component linearly depending on it can be written as time-independent functions:

$$\begin{aligned} \tilde{\sigma}(r,\varphi) &= C_\sigma(r)\cos\left(2\varphi - F_\sigma(r)\right), \\ \tilde{v}_r(r,\varphi) &= C_r(r)\cos\left(2\varphi - F_r(r)\right), \end{aligned} \tag{5}$$

where r is the galactocentric radius, φ is the azimuthal angle referenced to the large dynamical axis of the galaxy (Fig. 6c), C_i is the amplitude, and F_i is the phase of the ith parameter. To be specific, we consider the case of a two-arm galaxy.

Because the galaxy disk rotates differentially, the inner part of the disk (inside the corotation radius) rotates faster than the spiral pattern, while the outer part rotates more slowly (Fig. 8d). The observer at the corotation radius r_{c} notes that the direction of the disk angular velocity on the two sides of the corotation circle is opposite. According to (5), at each value of the radius, the perturbed surface density $\tilde{\sigma}(\varphi)$ changes sign four times (twice the number of spiral arms) with changing the azimuthal angle. Correspondingly, the radial velocity also changes sign four times. As a result, near the corotation region, where the total azimuthal velocity is small, closed azimuthal stream lines (vortices) emerge (Fig. 9a). Because the gas moves along the stream lines in

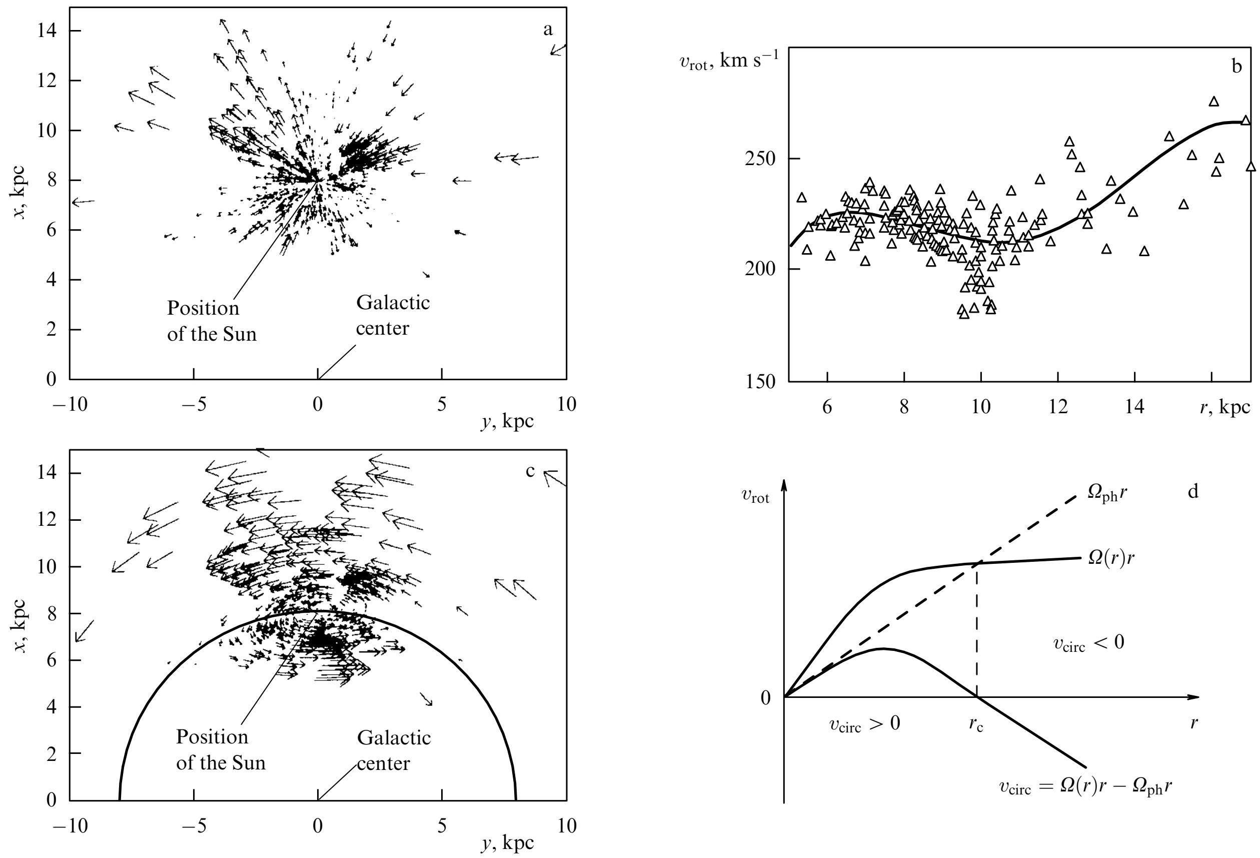

Figure 8. (a) The line-of-sight velocity field inferred from observations of a gas and stars [11]; the coordinates of the sun are (0, 8). (b) The circular rotation velocity as a function of the galactocentric distance r. The triangles indicate observational data, the solid line is the averaged rotation curve; near the position of the sun (8.5 kpc here), a velocity depression is observed [27]. (c) The model velocity field derived from gas and star motion [11]. (d) The transition from the inertial frame to the noninertial one rotating with the angular velocity of the spiral pattern Ω_{ph}. The solid curves show the unperturbed azimuthal velocity in the galaxy disk $\Omega(r)\,r$ for an observer at the galaxy center and the azimuthal velocity in the noninertial frame v_{circ} that vanishes at the corotation radius.

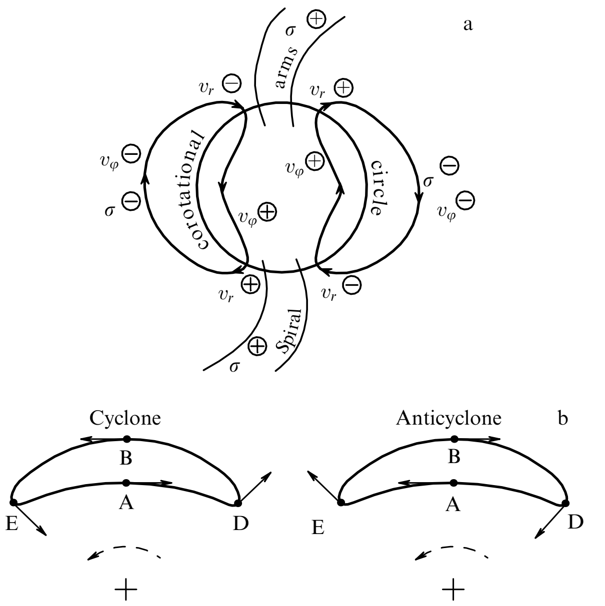

Figure 9. (a) The location of two anticyclones near the corotation radius in the frame corotating with a two-arm spiral pattern. The sign of the perturbed density σ changes four times at each radius along the azimuthal angle (the sign is plus on the arms and minus between them). (b) A schematic trajectory of particles; the arrow shows the direction of their motion in the cyclone and anticyclone.

the direction opposite to the disk rotation direction, these vortices are anticyclones (Fig. 9b).

We emphasize that these anticyclones cannot be treated as a mathematical peculiarity of the assumed rotation model in which the location of looped trajectories is fully determined by the frame angular velocity. The interstellar gas motion does not cross the spiral arms in the region of true corotation only. Therefore, the gas (if the velocity dispersion is small compared to the rotation velocity) is doomed to permanently flow either near a certain spiral arm or between the arms. The presence of vortex motions in the corotation region is a physical feature of galaxies. The evolution of star formation and gas content in the corotation region is of special interest, but lies beyond the scope of this review.

Thus, small perturbed velocities 'do their own job' in the entire disk by collecting matter into bright luminous arms, but in no way manifest themselves as being 'suppressed' by the large velocity of the disk. Only at the corotation radius, where the circular velocity of gas becomes small in the frame corotating with spiral arms, does the perturbed velocity take the form of giant anticyclones. This clearly demonstrates that spirals and vortices are different manifestations of one collective mechanism, called density waves.

The above qualitative picture of the formation of anticyclones in galaxy disks is based only on one assumption, the wave nature of the spiral structure. Therefore, vortex structures must be a universal attribute of spiral galaxies irrespective of the disk composition (gas or stars) and the density wave generation mechanism.

5.1 Location of centers of stationary vortices

Thus, we have shown that giant anticyclone vortices are real components of the large-scale structure of spiral galaxies. However, the interest in galaxy vortices is due not only to the presence of these new structures in spiral galaxies but also to the unique information that can be inferred from their analysis. A remarkable feature of giant anticyclones is the dependence of their centers relative to the spiral arms (Fig. 10a – c) on the wave structure formation mechanism.

The reason for such a dependence is obvious from general considerations. Indeed, the existence of stationary non-circular motions requires a certain balance of forces. The distribution of forces, in turn, is determined by the density distribution (spiral pattern) and by the type of forces (self-gravitation or pressure) that dominates.

To understand common dependences that determine the azimuthal location of vortices relative to the spiral arms, we consider regions where gas moves strictly along the radius (Fig. 10d). The distribution of the specific angular momentum, which is determined in the zeroth approximation by the rotation velocity of the disk, $M = \Omega r^2$, is inhomogeneous along the radius. As a result, the transition of a gas particle to another radius requires its angular momentum to change. This means that the azimuthal forces acting on the particle should 'spin up' or, inversely, 'spin down' its rotation, depending on whether the particle moves towards an increase or a decrease in the disk angular momentum. Figure 10d shows the direction of forces acting on a particle when the angular momentum increases with the radius.

The azimuthal force acting on a gas particle is determined by the azimuthal behavior of pressure perturbations $\widetilde{P}$ and the gravitational potential $\widetilde{\Phi}$ induced by the density wave, as well as by a possible external tidal force F_{ext} acting on the gas when the galaxy has a satellite or a strong bar:

$$F_{\varphi} = -\frac{1}{\rho r}\frac{\partial \widetilde{P}}{\partial \varphi} - \frac{1}{r}\frac{\partial \widetilde{\Phi}}{\partial \varphi} + F_{\text{ext}}. \qquad (6)$$

Therefore, if pressure forces dominate, the balance of forces needed for a stationary anticyclonic vortex to exist is established when the vortex center is located at the maximum of the perturbed pressure (Fig. 10e). The location of the pressure maximum in the spiral wave coincides with the density maximum, implying that the vortex is located on the spiral arm (Fig. 10a). The same relation is well known in meteorology: anticyclones in the terrestrial atmosphere are related to enhanced pressure regions, and cyclones correspond to low-pressure regions.

If the gas density in some region of the disk increases, test particles of the disk experience an additional gravitational attraction to this volume, i.e., the perturbed gravitational force is directed toward the enhanced density region (Fig. 10f). Consequently, if a spiral wave is of the gravitational nature and self-gravitation forces dominate in the corotation region, centers of anticyclones must be located at the density minimum, i.e., between spiral arms (Fig. 10b).

If external tidal forces are important in the corotation region, the centers of anticyclones do not coincide with either the density maximum or the density minimum (Fig. 10c).

If the specific angular momentum in the corotation region decreases with the radius (which is possible for a very steep decrease in the rotation speed), the direction of the azimuthal force, which is required for stationary anticyclones, changes to the opposite compared to that shown in Fig. 10d. The location of vortex centers relative to the spiral arms change accordingly (see the Table).

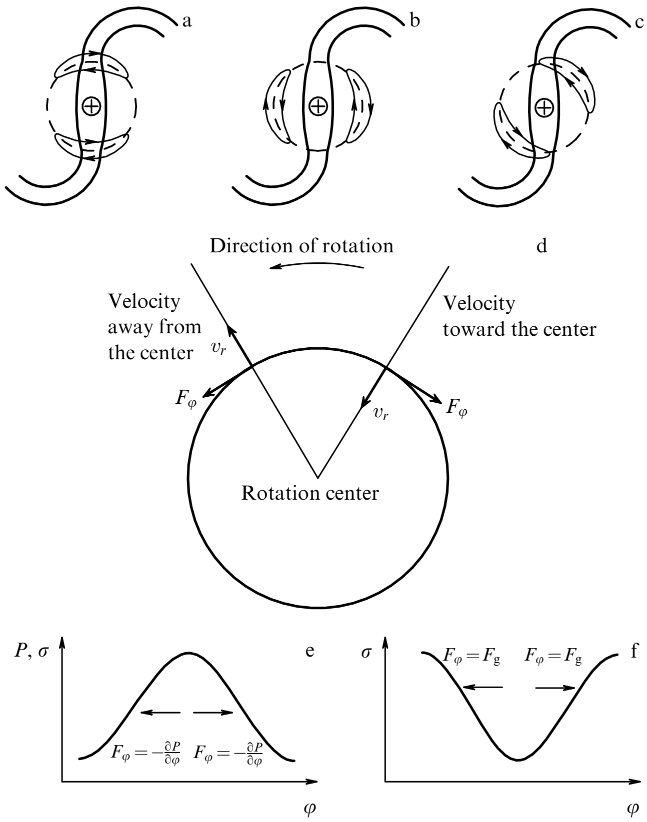

Figure 10. The location of vortices relative to spiral arms in a two-arm density wave: vortices on spirals (a), between spirals (b), and intermediate location of vortices (c). Thin solid lines with arrows indicate the motion of particles in vortices, thick solid lines show isodensity lines in spiral arms. If the disk angular momentum in the corotation region increases with the radius, the case shown in panel (a) corresponds to self-gravitation forces dominating, the case in panel (b) is realized when pressure forces dominate, and the situation shown in panel (c) is realized when tidal forces are significant at the corotation radius. For the angular momentum increasing with radius (d), if the radial velocity v_r is directed toward the center, the azimuthal force F_φ is directed against the rotation; if v_r is directed away from the center, F_φ is directed along the rotation. For azimuthal forces directed away from the vortex center, if dynamical pressure forces (the pressure gradient) prevail in the disk, maximum pressure and surface density should be attained at the vortex center (e); if gravitational force F_g dominates, the minimum of the surface density is attained at the vortex center (f).

Table. The vortex center location relative to spiral arms depending on the direction of the specific angular momentum growth and the dominant forces (hydrodynamic pressure or self-gravitation) in the disk.

Dominating force	Vortex center location	
	$\mathrm{d}M/\mathrm{d}r > 0$	$\mathrm{d}M/\mathrm{d}r < 0$
Pressure gradient	On the spiral	Between spirals
Self-gravitation	Between spirals	On the spiral
External gravitation force	Vortex center can be shifted with respect to the density extremum	

The existing data on the features of galactic anticyclones are fully consistent with the above analysis. The laboratory modeling in shallow water [9] was carried out in the case where a drastic decrease in the rotation speed was observed in the corotation region, which corresponds to the angular momentum decreasing with the radius, $\mathrm{d}M/\mathrm{d}r < 0$. Therefore, vortex structures were observed between spiral arms. Numerical simulations (see, e.g., [2]) showed that vortex structures also fall between spiral density arms in gaseous disks with sharp jumps in the rotation velocity. Indeed, in Mrk 1040, anticyclones were discovered to reside exactly between spiral arms (see Section 3). In [29], numerical modeling of the hydrodynamic instability generating spiral waves in disks with sufficiently smooth rotation curves, $\mathrm{d}M/\mathrm{d}r > 0$, was performed. Spiral structures were excited simultaneously with spiral arms and were located on them.

The problem of looped banana-like trajectories of stars in the gravitational field of a spiral wave corresponding to vortex structures in the stellar disk was considered in [30]. For small amplitudes of the spiral gravitational potential in disks with the angular momentum increasing along the radius, spiral structures were found to fall between the spiral arms. Thus, vortices in stellar and gaseous self-gravitating disks coincide (see the Table, the 'self-gravitation' row).

The question may naturally emerge: if vortex structures exist in all galaxies with spiral density waves and if their observation provides us with such invaluable information about the dynamical properties of a galaxy, why are we aware of only one or two phenomena with the observational signatures of such structures?

The reason is that vortex structures are much more difficult to discover than spiral ones. In the first case, one needs to solve a number of problems both purely observational and those related to methods of data processing. In particular, it is necessary to determine a fundamental parameter, the corotation radius of the spiral pattern.

As mentioned in Section 4, if the spiral structure is due to hydrodynamic instability at the velocity jump, the corotation radius coincides with the jump location. (We note that the observed jump in the rotation curve in some cases may not reflect the real peculiarity in changing the equilibrium rotation velocity with changing r, but can be due to the velocity field perturbation by a density wave.) However, if the rotation curve of a galaxy is smooth, the corotation radius cannot be found independently. In that case, as shown in [12], the full (three-dimensional) velocity field in the galaxy disk must be reconstructed in order to determine the corotation radius and to discover giant anticyclones.

5.2 How can three velocity components be determined from observations of one component?

The problem of restoring the full velocity vector stems from the fact that in astronomy, the velocity of a remote object is inferred from measurements of Doppler shifts of spectral lines. Therefore, only one velocity component along the line of sight is known. To reconstruct the other components of the velocity vector, a model of the object must be given.

As we see in what follows, one additional condition suffices for doing this. This condition assumes that for the galaxies under consideration, the perturbed surface density and velocity can be represented in terms of trigonometric functions [see also Eqn (5)]:

$$C(r)\cos\left[m\varphi - F(r)\right], \qquad (7)$$

where C and F are the amplitude and phase, and m is the azimuthal number equal to the number of the galaxy's arms.

To justify this assumption, we first note that the method, to be described in what follows, of reconstructing the total velocity vector field from the observed line-of-sight velocity field is valid only for galaxies with a grand-design spiral structure. These galaxies have a well-defined number of spiral arms, and hence their structure barely changes when rotating through the angle $2\pi/m$.

To validate assumption (7), we have offered several independent observational tests, which were applied to a number of grand-design spiral galaxies. In all cases, the possibility of describing the perturbed parameters of gaseous disks of galaxies in form (7) was confirmed.

We explain why such a simplified representation for $\widetilde{\sigma}$ and $\widetilde{v}$ can be quite accurate for real galaxies. The dynamics of gaseous galactic disks are described by the system of hydrodynamic equations. From this standpoint, approximation (7) means that, first, the system of equations describing the behavior of grand-design galaxies is almost linear. Second, the general solution of this system (which can be represented in the form of a Fourier series in azimuthal harmonics) is dominated by the term corresponding to one harmonic with the azimuthal number m.

As regards the correctness of the linear approximation for the hydrodynamic description of gaseous galactic disks, we note that the perturbed velocities (20 – 30 km s^{-1}) are small compared to the unperturbed rotation speed ($>$ 200 km s^{-1} as a rule) in these galaxies. We also note that the Fourier series of axially nonsymmetric perturbations of the surface brightness of these galaxies point to the dominance of the second harmonic in the perturbed surface density.

According to theoretical studies [31, 32], nonlinear effects stabilize the instability that already shapes the observed structures for small amplitudes of the perturbed quantities when the linear approximation is still valid in describing the relations between different parameters of the perturbation. In the final state, the harmonic with the initially maximum increment then dominates.

Although all physical theories require experimental justification, theory and experiment develop independently as a rule. In our case, this inconsistency was manifested in that the problem of discovering giant anticyclones in galaxies was posed earlier than technological possibilities for solving it appeared.

Initial attempts to find vortices in the velocity fields of gaseous galactic disks used the data available at that time — one-dimensional distributions of line-of-sight velocities along a spectrograph slit for different slit orientations. But such an approach was not accurate enough to distinguish vortices: the line-of-sight velocities should be known at several thousand points of the disk with the accuracy up to a few kilometers per second. The situation changed only recently.

Significant progress in observations of the line-of-sight velocity fields of gaseous disks of external galaxies has been achieved in the last 5 – 10 years. Currently, we are able to measure line-of-sight velocities simultaneously at 10,000 (or even more) points of the disk. For ionized gas regions, the accuracy of an individual line-of-sight velocity measurement can be as high as $\sim$ 5 km s^{-1}; for neutral gas, it is $\sim$ 2 km s^{-1} (by means of radio observations).

The typical line-of-sight velocity fields of the gas in spiral galaxies are shown in Fig. 11 a (the galaxy NGC 157) and

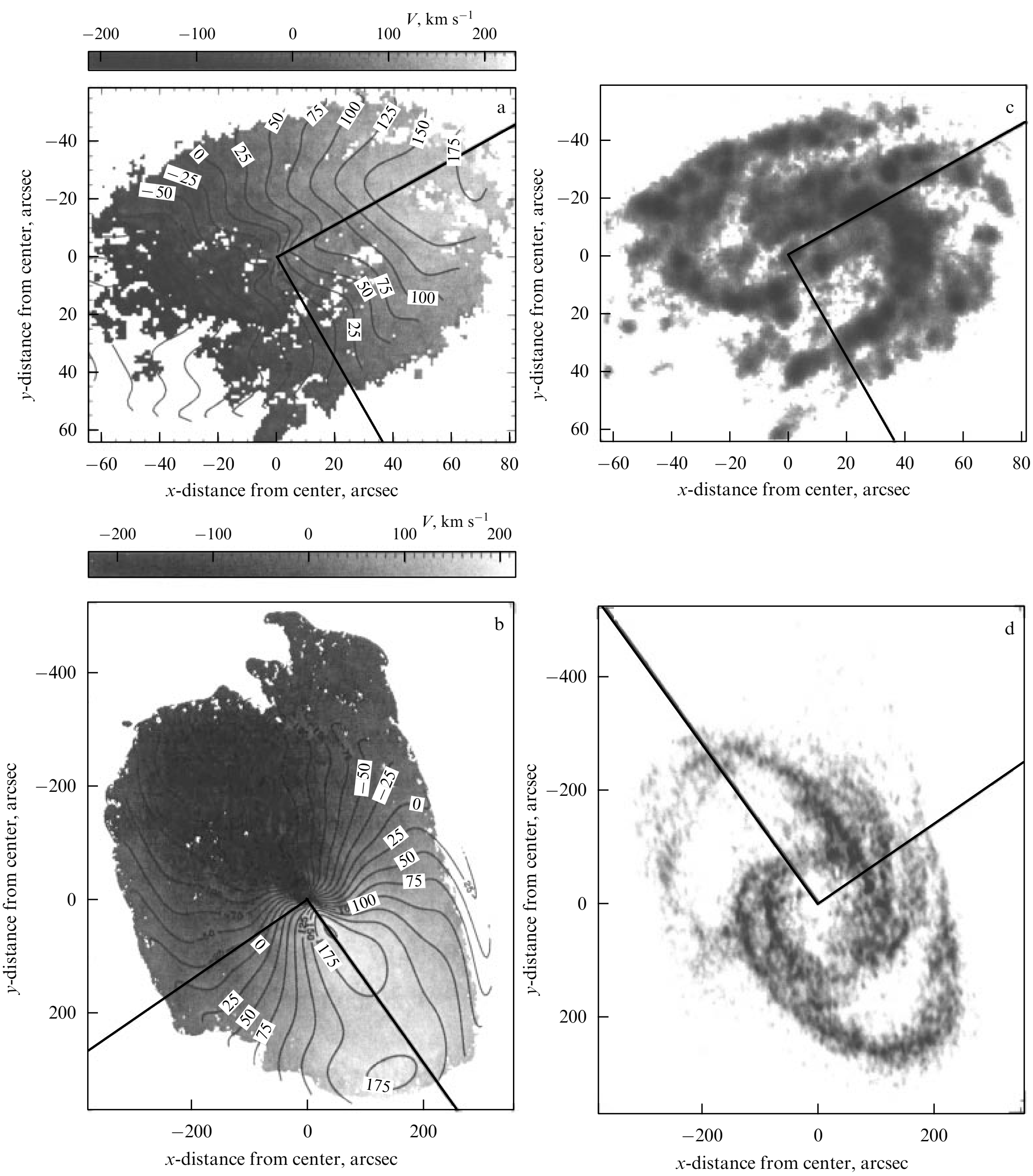

Figure 11. Line-of-sight velocity fields of NGC 157 (a) and NGC 1365 (b) obtained by the Doppler shift in the Hα and 21-cm (HI) lines, respectively, with isoline values indicated. Surface brightness maps of NGC 157 in the Hα line (c) and NGC 1365 in the 21-cm line (d).

Fig. 11b (the galaxy NGC 1365). In Fig. 11c, d, we show the brightness maps for these galaxies.

Studies of the velocity fields in spiral galaxies showed that perturbed velocities in spiral arms are much less than circular velocities. This allows applying linear and quasi-linear theories for analysis.

According to the linear theory, density waves with a certain value of the azimuthal number should emerge in galaxy disks. It can then be shown that all three velocity components in a flat disk must contribute to different Fourier harmonics of the observed line-of-sight velocity. The main idea of reconstructing the full velocity vector is very simple. First, the Fourier coefficients of the line-of-sight velocity field must be determined from observations, and then all three velocity components of gas in the galaxy are to be found using simple algebraic relations. In the framework of this theory, phase relations between different velocity components turn out to exhibit jumps at the corotation region. Therefore, restoring all three velocity components automatically solves the problem of determining the spiral pattern corotation radius.

We consider how to determine the velocity components in more detail. We first find the relation between the observed line-of-sight velocity of a gas cloud C moving in the galaxy disk and three velocity components.

We first consider the simplest case where the inclination angle of the galaxy is $i = \pi/2$ (Fig. 12). The observer measures only the component of the velocity of point C directed along the line of sight, i.e., the velocity component along the z' axis. The azimuthal and radial components of the velocity

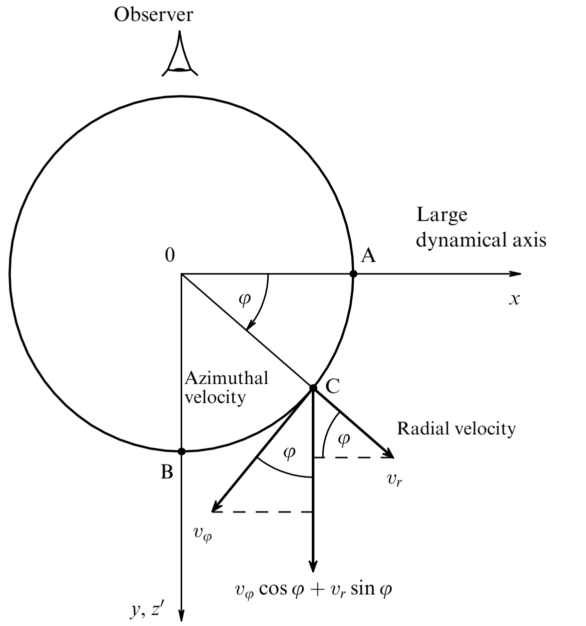

Figure 12. The case of an edge-on galaxy (the inclination angle of the galaxy is $\pi/2$). The observed line-of-sight velocity of point C is $v_{\rm obs} = v_{\rm sys} + v_\varphi \cos\varphi + v_r \sin\varphi$, where $v_{\rm sys}$ is the systematic velocity of the galaxy along the line of sight.

contribute $(v_\varphi)_{z'} = v_\varphi \cos\varphi$ and $(v_r)_{z'} = v_r \sin\varphi$, respectively. The component of the systematic velocity of the entire galaxy along the line of sight $v_{\rm sys}$ must also contribute. The vertical (perpendicular to the galaxy plane) velocity component v_z does not contribute to the measured velocity at $i = \pi/2$. As a result, the line-of-sight velocity at $i = \pi/2$ is expressed in terms of the velocity components as

$$v_{\rm obs} = v_{\rm sys} + v_\varphi \cos\varphi + v_r \sin\varphi\,.$$

For an arbitrary galaxy inclination angle, we have

$$v_{\rm obs} = v_{\rm sys} + (v_r \sin\varphi + v_\varphi \cos\varphi)\sin i + v_z \cos i\,.$$

For a density wave with a fixed azimuthal number, the perturbed density $\widetilde{\sigma}$ and velocities $\widetilde{v}_r$, $\widetilde{v}_\varphi$, and $\widetilde{v}_z$ can be represented as

$$\widetilde{\sigma}(r,\varphi) = C_\sigma(r)\cos\left[m\varphi - F_\sigma(r)\right], \tag{8}$$

$$\widetilde{v}_r(r,\varphi) = C_r(r)\cos\left[m\varphi - F_r(r)\right], \tag{9}$$

$$\widetilde{v}_\varphi(r,\varphi) = C_\varphi(r)\cos\left[m\varphi - F_\varphi(r)\right], \tag{10}$$

$$\widetilde{v}_z(r,\varphi) = C_z(r)\cos\left[m\varphi - F_z(r)\right]. \tag{11}$$

Now, if we take velocities in the galaxy disk as the sum of perturbed and unperturbed components,

$$\begin{aligned} v_r(r,\varphi) &= \tilde{v}_r(r,\varphi)\,,\\ v_\varphi(r,\varphi) &= v_{\rm rot}(r) + \tilde{v}_\varphi(r,\varphi)\,,\\ v_z(r,\varphi) &= \tilde{v}_z(r,\varphi)\,, \end{aligned} \tag{12}$$

and substitute the full velocities in the formula for $v_{\rm obs}$, we obtain the decomposition of the observed velocity in a Fourier series in the azimuthal angle φ. The series includes eight terms describing the zeroth harmonic proportional to $v_{\rm sys}$, the first even harmonic proportional to $v_{\rm rot}$, as well as even and odd $(m-1)$th, mth, and $(m+1)$th harmonics. The corresponding Fourier coefficients are

$$a_{m-1} = \frac{C_\varphi \cos F_\varphi + C_r \sin F_r}{2}\,\sin i\,, \tag{13}$$

$$b_{m-1} = \frac{C_\varphi \sin F_\varphi - C_r \cos F_r}{2}\,\sin i\,, \tag{14}$$

$$a_{m+1} = \frac{C_\varphi \cos F_\varphi - C_r \sin F_r}{2}\,\sin i\,, \tag{15}$$

$$b_{m+1} = \frac{C_\varphi \sin F_\varphi + C_r \cos F_r}{2}\,\sin i\,, \tag{16}$$

$$a_m = C_z \cos F_z \cos i\,, \tag{17}$$

$$b_m = C_z \sin F_z \cos i\,. \tag{18}$$

Other coefficients of the Fourier decomposition of $v_{\rm obs}$ are zero. The above relations show that different components of gas velocity in a galaxy contribute to the azimuthal Fourier harmonics of the observed line-of-sight velocity as follows:

- the systematic velocity of the galaxy contributes to the zeroth harmonic of the observed velocity;
- the velocity of the purely circular motion determines the coefficient at the cosine of the first harmonic of the observed velocity;
- the radial and azimuthal components of the velocity contribute to the $(m-1)$th and $(m+1)$th harmonics of the observed velocity;
- the vertical velocity determines the mth harmonic of the observed velocity.

Thus, if there are m spiral arms in the galaxy, the line-of-sight velocity field must have the $(m-1)$th and $(m+1)$th harmonics in addition to the zeroth and first ones.

Deriving the Fourier coefficients of the velocity field from observations, we find the parameters of the vector velocity field in the galaxy from the system of equations (13)–(18).

Indeed, in this case, it is easy to see that eight Fourier coefficients are nonzero, which is just enough to determine the eight unknown functions $v_{\rm sys}$, $v_{\rm rot}$, C_r, C_φ, C_z, F_r, F_φ, and F_z. The problem of reconstructing three velocity components from the observed line-of-sight velocity field can thus be solved for galaxies with the number of arms $m \geqslant 3$.

For a two-arm galaxy, only seven Fourier coefficients can be derived: $a_0, a_1, a_2, a_3, b_1, b_2, b_3$. One more equation relating unknown functions is required.

We proposed three independent methods of restoring three velocity components using different types of additional relations between the density wave parameters. The first two are based on relations between phases of unknown functions obtained from hydrodynamic equations with a single assumption: the perturbation is represented as a wave with the azimuthal number $m = 2$.

The first method is based on the fact that for comparatively smooth rotation curves (such that $\varkappa^2 \equiv 2\Omega\,(2\Omega + r\,{\rm d}\Omega/{\rm d}r) > 0$), the phases of radial and azimuthal velocities must be related (before and after the corotation radius $r_{\rm c}$) as

$$\begin{aligned} F_\varphi - F_r &= -\frac{\pi}{2} \quad \text{at} \quad r < r_{\rm c}\,,\\ F_\varphi - F_r &= \frac{\pi}{2} \quad \text{at} \quad r > r_{\rm c}\,. \end{aligned} \tag{19}$$

For a sharply changing rotation curve ($\varkappa^2 < 0$), the following relations hold:

$$F_\varphi - F_r = \frac{\pi}{2} \quad \text{at} \quad r < r_c\,,$$
$$F_\varphi - F_r = -\frac{\pi}{2} \quad \text{at} \quad r > r_c\,. \tag{20}$$

The second method is based on the fact that for tightly wound spirals, the phases of azimuthal and radial velocities must satisfy the relations

$$F_r - F_\sigma = \pi \quad \text{at} \quad r < r_c\,,$$
$$F_r - F_\sigma = 0 \quad \text{at} \quad r > r_c\,. \tag{21}$$

These jumps in the phase difference allow the corotation radius of the spiral structure to be determined directly from the line-of-sight velocity field observations.

The third method consists in determining the equilibrium rotation curve as inferred from the mass distribution in the galaxy. This method is based on studies of the photometric brightness distribution in galaxies.

Only one question remains: What do different restoration methods and tests of their validity give for real galaxies?

6. Discovery of anticyclones in spiral galaxies with smooth rotation curves

6.1 On the possibility of approximating real spiral perturbations in galaxies by monochromatic low-amplitude waves

As follows from Section 5, the first step in restoring the full velocity field of gaseous galaxy disks consists in testing, for real grand-design galaxies, the validity of a simplified description in the form of monochromatic perturbations (8)–(11). Most spiral galaxies have two arms. The test therefore includes two parts:

• testing the amplitude closure of the second harmonic in the surface density Fourier spectrum;

• testing the amplitude closure of the first three harmonics in the line-of-sight velocity field Fourier spectrum [see relations (13)–(18)].

Figure 13 shows spectra of the surface brightness maps of the galaxy NGC 157 in the near-infrared (K) range (Fig. 13a) and NGC 1365 on the 21 cm neutral hydrogen line (Fig. 13b). As can be seen from the figure, the second harmonic of the surface brightness clearly dominates in both galaxies, which means that the same harmonic dominates in the surface density spectrum $\tilde{\sigma}$.

The appearance of the first three harmonics in the line-of-sight velocity spectrum is a consequence of the projection effect. From the mathematical standpoint, this happens due to the multiplication of the monochromatic components of the gas velocity vector, depending on 2φ, with similarly monochromatic functions of the argument φ ($\cos\varphi$ and $\sin\varphi$), when making a projection on the line of sight. Therefore, testing the prevalence of the first three harmonics in the line-of-sight velocity spectrum is, in essence, the test of the amplitude closure of the second harmonics in the velocity vector components v_r, v_φ, v_z.

Figure 13c, d shows the Fourier spectra of the line-of-sight velocity fields of galaxies NGC 157 and NGC 1365 without

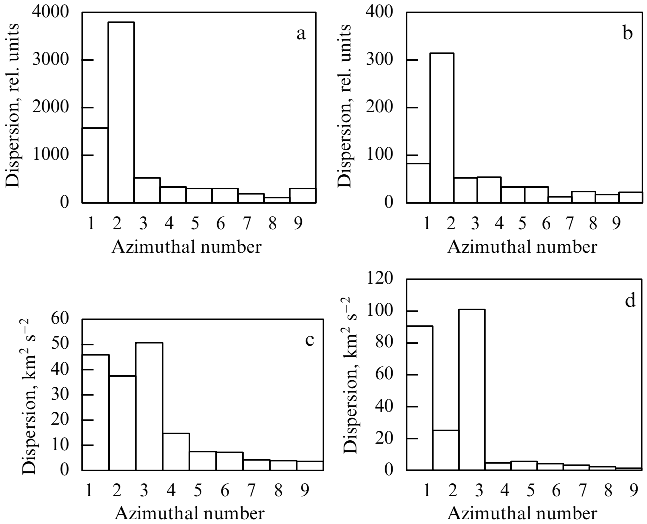

Figure 13. Fourier spectra of the axially nonsymmetric part of the surface brightness maps of NGC 157 in the K-band (a) and of NGC 1365 on the 21 cm line (b). Fourier spectra of the line-of-sight velocity fields of NGC 157 (c) and NGC 1365 (d) presented in Fig. 11.

contributions from the systematic velocity and the purely circular gas motion (more precisely, the contribution from the first even harmonic). The first of the fields is obtained in the line of ionized hydrogen Hα, and the second in the line of neutral hydrogen 21 cm. In both cases, the first three harmonics clearly dominate, which confirms the good accuracy of describing real spiral perturbations in galaxies as monochromatic.

6.2 Observational test: do spiral arms represent density waves?

The test presented in Section 6.1 is evidence of the possibility of describing real spiral perturbations by one Fourier harmonic. This property allows restoring the full vector velocity field of gas from a one-component line-of-sight velocity field (see Section 5). But the velocity field reconstructed in this way can turn out to be only 'the instant image,' revealing little about complicated processes in the galaxy disk. Nevertheless, if the spiral perturbation is in the form of a density wave, the situation changes dramatically: after passing to the frame corotating with the spiral pattern, the reconstructed field proves to be stationary and fully characterizes the dynamical state of the disk.

Thus, we arrive at the necessity of observational tests of whether the spiral structure of a given galaxy represents a density wave. We mentioned in Section 2 that Lindblad's hypothesis on the wave nature of spiral waves resolved the paradox of the nonsmearing of the spiral structure by differential rotation. In Section 4, we presented an observational test of the hypothesis on the wave nature of the spiral arm in our Galaxy — the change in the sign of the gradient of stellar ages on the corotation circle inside the spiral arm (see Fig. 7). We also noted that this test can be applied only in the solar vicinity of our Galaxy. What about the observational tests of the wave nature of spiral arms in other galaxies?

In this section, we outline one observational test we proposed to establish the wave nature of galactic spiral arms [11, 12]. In this method, in addition to the theory of characteristic disk oscillations, we also use the relation between the observed line-of-sight velocity of the gaseous disk and perturbed gas velocity components. Equations (15) and (16) imply a relation between the third harmonic of the observed velocity $v_{\rm obs}$ and wave motions in the disk plane only, i.e., only with two components of the perturbed gas velocity, $\widetilde{v}_r$ and $\widetilde{v}_\varphi$. This means that some functional dependence exists between the third harmonic of the line-of-sight velocity F_3 and phases F_r and F_φ, which can be written as

$$F_3 = f_1(F_r, F_\varphi)\,. \tag{22}$$

However, as follows from the theory of eigenoscillations of a disk, the phases F_r and F_φ are not independent but are related by Eqns (19) or (20), depending on the sign of $\varkappa^2$. Therefore, functional dependence (22) simplifies:

$$F_3 = f_2(F_r)\,. \tag{23}$$

From Eqns (21), we can find a single-valued dependence between phases F_r and F_σ. Therefore, we finally obtain

$$F_3 = f(F_\sigma)\,. \tag{24}$$

Because the second harmonic dominates in the surface brightness Fourier spectrum (Fig. 13a, b), the phase F_σ in fact coincides with the phase of the second harmonic of the brightness. The latter can be easily obtained from observations. The phase F_3 in Eqn (24) can also be calculated as the phase of the third Fourier harmonic of the observed line-of-sight velocity $v_{\rm obs}$.

Thus, Eqn (24) can easily be verified, which represents the observational test of the wave nature of the spiral structure.

According to [11, 12], Eqn (24) can be explicitly written as

$$\Phi \equiv F_3 - \frac{\pi}{2} = F_\sigma \quad \text{for} \quad r > r_{\rm cr}\,, \tag{25}$$

$$\Phi \equiv F_3 - \frac{\pi}{2} = F_\sigma \quad \text{for} \quad r < r_{\rm cr}, C_\varphi > C_r\,, \tag{26}$$

$$\Phi + \pi \equiv F_3 + \frac{\pi}{2} = F_\sigma \quad \text{for} \quad r < r_{\rm cr}, C_\varphi < C_r\,. \tag{27}$$

The fulfillment of conditions (25)–(27) for a real galaxy implies, as was already noted, that its spiral arms are density waves.

The verification of the observational test described above can be given a visually clear form by taking into account that for galaxies satisfying the condition $C_\varphi > C_r$, two curves determined by the equations

$$\cos(2\varphi - F_\sigma) = 1\,, \tag{28}$$

$$\cos(2\varphi - \Phi) = 1\,, \tag{29}$$

according to formulas (25) and (26), must coincide everywhere in the disk. Equation (28) then defines the curve of the maximum of the surface brightness second harmonic, and Eqn (29) defines the test curve describing a two-arm spiral with the line-of-sight velocity phase of the third Fourier harmonic F_3 shifted by $\pi/2$.

For galaxies that are characterized by the inverse relation, $C_\varphi < C_r$, both curves (28) and (29) must coincide outside the corotation circle, $r > r_{\rm c}$. In the region $r < r_{\rm c}$, the test curve must coincide with the curve of the minimum of the surface brightness second harmonic. In other words, for $C_\varphi < C_r$, the test curve must have a jump at the corotation region in passing, roughly speaking, between the spiral arms inside the corotation circle, and after changing its location in the jump, must become coincident with the spiral arm (with the curve of the brightness maximum) outside the corotation circle.

This correlation of curves can be seen in Fig. 14, where the triangles mark the curve (29). The squares in Fig. 14a show the curve of the maximum of the surface brightness second harmonic in the K-band of the galaxy NGC 157, for which $C_\varphi > C_r$. Good coincidence of the curves is evident. Figure 14b, c shows the comparison of the lines of the maxima of the second harmonic in the R band, with maxima and minima of the test curve for the galaxy NGC 3631. For this galaxy, at $10'' < r < 50''$, the amplitude of the perturbed azimuthal velocity is smaller than the amplitude of the perturbed radial velocity, $C_\varphi < C_r$ [33]. It is seen that maxima of the test curve coincide with maxima of the surface brightness in the central part of the disk and outside the corotation circle. In the intermediate region, they almost

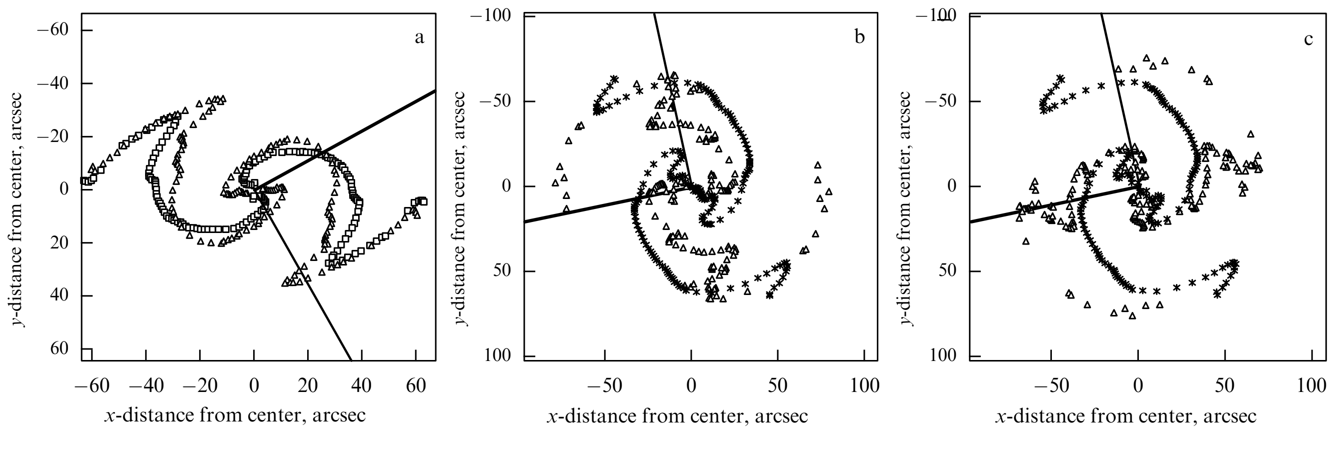

Figure 14. (a) The galaxy NGC 157 characterized by the condition $C_\varphi > C_r$. Shown is the superposition of the surface brightness second harmonic maximum in the K-band (squares) described by Eqn (28) and of the test curve (triangles) described by Eqn (29). (b, c) The galaxy NGC 3631, for which $C_\varphi < C_r$ for $10'' < r < 50''$ [33]. Shown is the superposition of the following curves: the location of the surface brightness second harmonic maximum in the red (R) band (asterisks), the location of maxima of the test curve (triangles in panel b), and the location of minima of the test curve (triangles in panel c).

coincide with minima of the surface brightness, as should be the case for a galaxy with $C_\varphi < C_r$. Therefore, the wave nature of the spiral structure can be established in the galaxy NGC 3631 as well. It follows from the above that spiral arms of the galaxies are indeed density waves.

6.3 Vertical motions in gaseous disks of spiral galaxies: vertical velocities in the spiral density wave or bending oscillations?

The test considered in Section 6.2. proves the relation between the two-arm density wave and the first and third harmonic of the line-of-sight velocity field caused by motions in the disk plane. Exactly these motions are of primary interest for us from the standpoint of distinguishing giant anticyclones similar to those observed in shallow-water experiments. However, to be able to restrict ourself by taking only these harmonics into account, we must show that the second Fourier harmonic is produced by vertical motions in the same density wave. In this section, we show an example of using one of the observational tests proposed by us for this purpose [34].

To clarify the main idea of this observational test, we recall some statements from the theory of galaxy disk oscillations.

Two types of vertical motions in galaxy disks excited by quite different mechanisms are known [35]. The first type is related to density waves and, together with motions in the disk plane (which we have already considered), constitutes one three-component vector velocity field in the spiral density wave. This type of motion does not deform the central disk plane $z = 0$ because the velocity component v_z in the density wave is an odd function of z: $v_z(-z) = -v_z(z)$, such that $v_z = 0$ in the plane $z = 0$.

The second type of vertical motions leads to disk bending like the surface of an oscillating membrane. The vertical velocity in such a motion is an even function of the coordinate z transversal to the disk plane: $v_z(-z) = v_z(z)$ and $v_z \neq 0$ in the plane $z = 0$. Such a behavior of the gaseous disk can be caused by either tidal influence from a satellite galaxy or the appropriate motion of the star disk in which the gaseous disk is embedded.

In a star disk, the membrane (bending) oscillations are excited by the so-called hose-pipe instability emerging when the velocity dispersion of stars in the disk plane is much higher than in the vertical direction. In this case, a small initial bending of the disk is enhanced by the centrifugal force acting on stars moving along curved trajectories. In the same way, centrifugal forces bend a fire-hose with rapidly flowing water, from which the name of this instability originated.

Therefore, we must understand which type of vertical motions, differing by the class of symmetry of the function $v(z)$ relative to the plane $z = 0$, is observed in the gas disk of spiral galaxies and is responsible for the appearance of the second harmonic in the Fourier spectrum of the line-of-sight velocity field. To solve this problem, it is natural first of all to choose a galaxy oriented to the observer such that the vertical velocity $v(z)$ mostly contributes to the observed velocity along the line of sight. Then we should measure the line-of-sight velocity such that the results differ for different symmetries of $v_z(z)$.

The first requirement is satisfied if the galaxy is seen under a small inclination angle i (so-called 'face-on' galaxies), because the ratio of contributions of the vertical velocity and the velocity in the disk plane are proportional to $\cos i$.

As a method sensitive to the v_z symmetry, we can use the comparison of results of measurements of one vertical velocity field at different wavelengths for different transparencies of the gaseous disk. The optical depth of the disk should be less than unity in one band and larger than unity in the other band. These requirements are satisfied, for example, for velocity measurements using the Doppler shift of the 21 cm line and the Hα line.

We explain what kind of differences in the results of measurements can be expected using different wavelengths in a disk with different optical depth and different types of vertical gas motions in the galaxy disk.

On the Hα line, due to the large optical depth in this line, we mostly observe the nearest part of the disk. Therefore, measurements on the Hα line yield the maximum vertical velocity for both types of vertical motions. Indeed, an odd v_z is equal to zero in the plane $z = 0$ and increases farther away from this plane, reaching maximum at the disk edge, i.e., where we measure it on the Hα line. The value of v_z in bending oscillations is virtually independent of z (up to the factor $2\pi z/\lambda \ll 1$, where λ is the wavelength [35]).

For observations on the 21 cm line, where the disk is almost transparent, contributions from the disk parts located on opposite sides of the central plane $z = 0$ are approximately equal. For an odd $v_z(z)$, these contributions mutually cancel — parts with opposite vertical velocities cause the opposite Doppler line shift and the maximum of this function is not shifted. Therefore, for vertical motions in the density wave, the line-of-sight velocity (with the systematic velocity of the galaxy subtracted) measured in the 21 cm line is much smaller than measured in the Hα line. For membrane oscillations and even $v_z(z)$, measurements on both lines should be similar, i.e., virtually coincide.

The outlined observational method for determining the nature of vertical motions in galaxy disks has been verified in studies of the velocity field of the spiral galaxy NGC 3631, which displays a distinct two-arm structure (Fig. 15a) and is seen almost 'face-on' ($i = 17°$). This galaxy is isolated, which excludes its tidal deformation.

Observations on the Hα line used in the present study were obtained by the 6 m telescope of SAO RAS [33, 34]. Observations on the 21 cm line were carried out by Knappen at the Westerbork Synthesis Radio Telescope [36]. The optical (Hα) and radio (21 cm) observations had significantly different angular resolutions ($2''$ and $15.2'' \times 11$) for technical reasons. For a more adequate comparison, we therefore smoothed the optical velocity field to the resolution $13''$, comparable to that of radio data. The original optical field, smoothed optical field, and radio field of the line-of-sight velocity in the galaxy NGC 3631 are shown in Fig. 15b, c, d.

The Fourier spectra of all the fields shown in Fig. 15b – d demonstrate the prevalence of the first three harmonics (Fig. 15e – g), which is a consequence of the two-arm spiral structure of this galaxy [see Eqns (13) – (18)].

The results presented in Fig. 15e – g are consistent with the assumption that the second Fourier harmonic of the line-of-sight velocity field is due to gas vertical motions in the disk of NGC 3631. Indeed, for the Hα data shown in Fig. 15e, f, only the second harmonic has an appreciable amplitude, as should be the case if this harmonic is due to vertical motions, whereas the first and third harmonics are due to motions inside the disk plane. The contributions of these harmonics prove to be suppressed by the projection effect (the projection of these

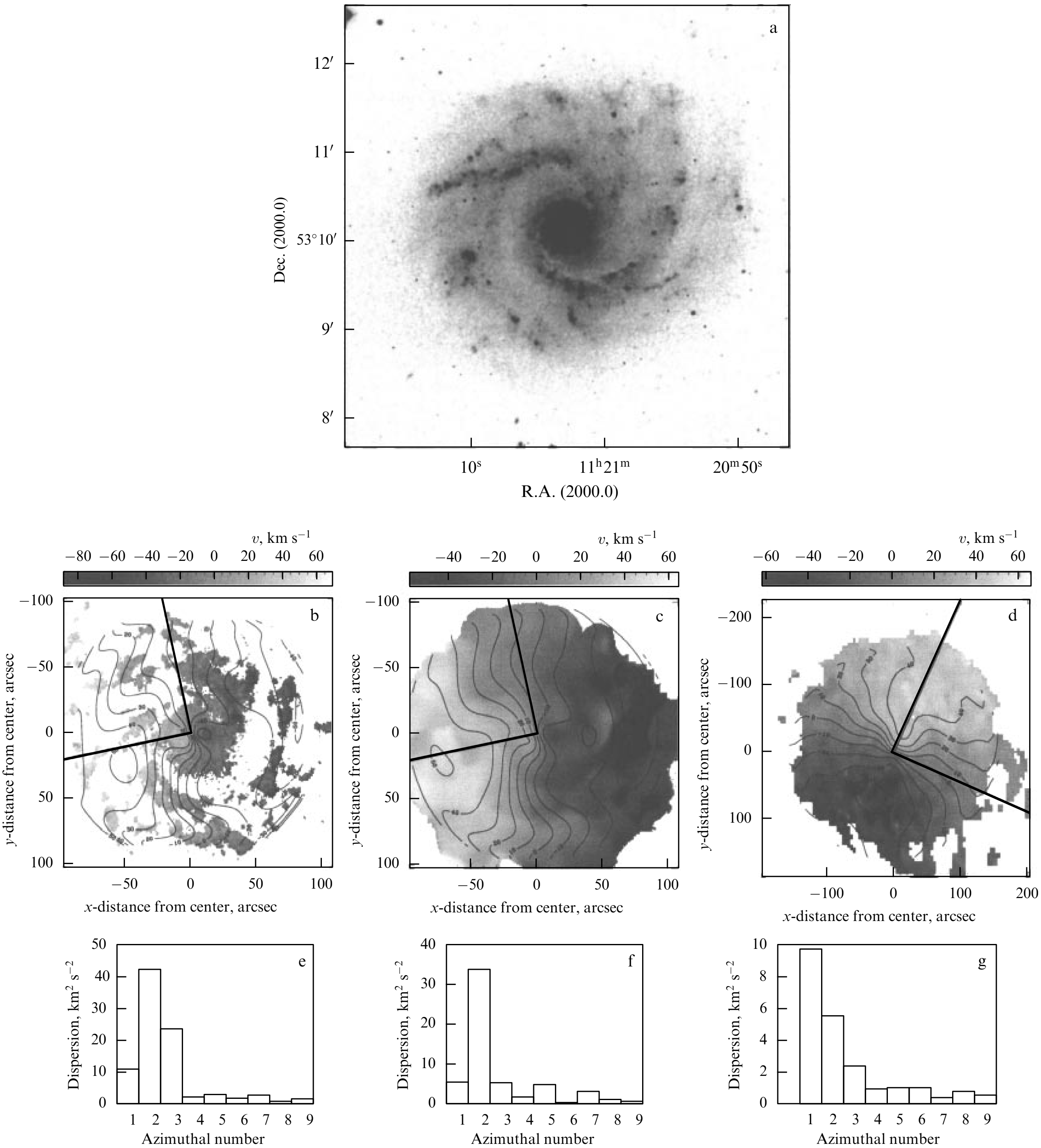

Figure 15. The image of the spiral galaxy NGC 3631 in the R-band (from the Isaac Newton Telescope archive, Canary Islands) (a). Line-of-sight velocity fields of gas in this galaxy as measured on the Hα line with the high angular resolution $\approx 2''$ (b) or smoothed to the angular resolution $\approx 2''$ (c), and on the 21 cm line with the resolution $15.2 \times 11''$ (d). The contribution of different Fourier harmonics to the deviation of the line-of-sight velocity field of this galaxy from purely circular motion, averaged over the disk region ($r < 80''$): (e) — the velocity field on the Hα-line with high angular resolution, (f) — smoothed velocity field on the Hα line, (g) — the velocity field on the 21 cm line.

velocities on the line of sight is proportional to $\sin i$). For NGC 3631, $\sin i \simeq 0.3$. (The dispersion measured in units of [km^2 s^{-2}] shown in Fig. 15e – g is suppressed even more strongly because it is proportional to $\sin^2 i \simeq 0.1$.) At the same time, the amplitude of the second harmonic of the line-of-sight velocity field as inferred from the radio data is much lower (Fig. 15g).

Comparing Figs 15e, f, and g, we conclude that the smaller amplitudes of the first and third harmonics of the velocity field on the 21 cm line in comparison with ones of the original field on the Hα line are related to the resolution effect, these harmonics have similar amplitudes in the line-of-sight velocity field observed on the 21 cm line (Fig. 15g) and in the smoothed velocity field on the Hα line. The second harmonic on the 21 cm radial velocity field is much smaller than in the smoothed velocity field on the Hα line (Fig. 15f). This suggests that not bending oscillations but vertical motions in the density wave are observed in NGC 3631 [33, 34].

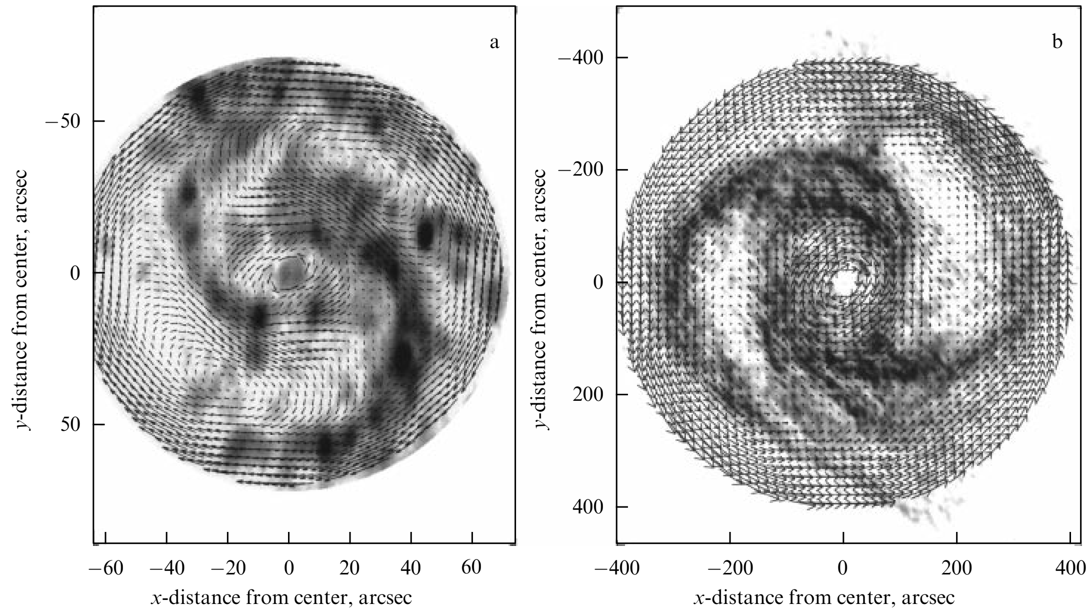

Figure 16. The gas velocity field in the galaxy plane for NGC 157 (a) superimposed on its surface brightness map on the Hα line and NGC 1365 (b) superimposed on its surface brightness map on the 21 cm line.

6.4 Gas velocity field in the galaxy disk plane

As follows from Sections 6.1 – 6.3, all independent observational tests confirm the applicability of our method of restoring the full vector field of gas velocities in spiral grand-design galaxies from the observed line-of-sight velocity field.

So far, we have processed the observed line-of-sight velocity fields and reconstructed the full velocity vector for about ten spiral galaxies, including NGC 157, NGC 6148, NGC 1365, and NGC 3893 [11, 33, 37 – 40]. In all cases, independent methods yielded consistent results. This allowed us to reach quite a different level of proof of the obtained results. In astronomy (with the exception of the nearest objects in the solar system), it is impossible to 'touch' objects under study or perform experiments with them, as is common in physics. The coincidence of results obtained by independent means of analysis of observational data can lend support to the model used.

Having an error in the velocity measurements of one pixel in an image of about 15 km s^{-1} and using more than 10^5 velocity determinations, we have managed to detect the velocity amplitude 20 – 30 km s^{-1} in spiral arms with the accuracy 2 – 5 km s^{-1}.

The velocity reconstruction allows resolving two classic problems simultaneously: to determine the corotation radius and to directly prove the wave structure of the observed spiral arms. Moreover, this method enabled us to solve new problems. One of the most important problems is the discovery of new structures in galaxies — giant anticyclones.

For two galaxies NGC 157 and NGC 1365, Fig. 16 shows velocity fields in the gaseous disk plane in the frame corotating with a spiral pattern, superposed on the deprojected images of the corresponding galaxies. If the spiral pattern is stationary or quasi-stationary, this velocity field is also stationary or slowly varying with time. In Fig. 16, two very distinct anticyclones are observed near the corotation radius in either case. Such anticyclone vortices were predicted from laboratory shallow-water experiments. The centers of the anticyclones lie on the corotation radius.

We note that perturbed gas velocities in spiral arms are directed toward the galaxy center within the corotation radius and outward from the galaxy center beyond the corotation radius. Such behavior of velocities is predicted by the theory of the density wave.

The comparison of the location of spiral arms with that of anticyclones shows that the center of the anticyclones lies in the interarm space, implying that self-gravitation forces in gas exceed hydrodynamic pressure forces for the chosen galaxies (see the Table).

An analysis similar to the one presented here can presently be performed for only a very limited number of galaxies. But it clearly demonstrates the great possibilities opened by analyzing the Fourier components of the azimuthal distribution of the line-of-sight velocity whenever appropriate observational data are available.

Despite the common nature of the spiral-vortex structure, vortices were discovered one and a half century after spiral arms. Spiral arms are as bright as the 'tip of an iceberg,' striking astronomers by the diversity and dynamical character of their forms. Vortices turned out to be the 'underwater' part of the same 'iceberg,' which cannot be discovered by many telescopes at very different wavelengths. The reason for this was not the insufficient power of the telescopes but the need to invoke the predictive power of laboratory and numerical modeling and to carry out analytic studies to reveal the nature of these hidden structures, their localization, and the means by which they can be inferred from observations. Long-term efforts to search for these structures now allow obtaining the dynamic picture of spiral galaxies, which we could not have even imagined at the beginning of this work.

7. Prediction and discovery of giant cyclones

As noted in Section 5 (Fig. 7e and 8a), in the frame corotating with spiral arms, the directions of disk rotation inside and outside the corotation circle are opposite (solid lines with

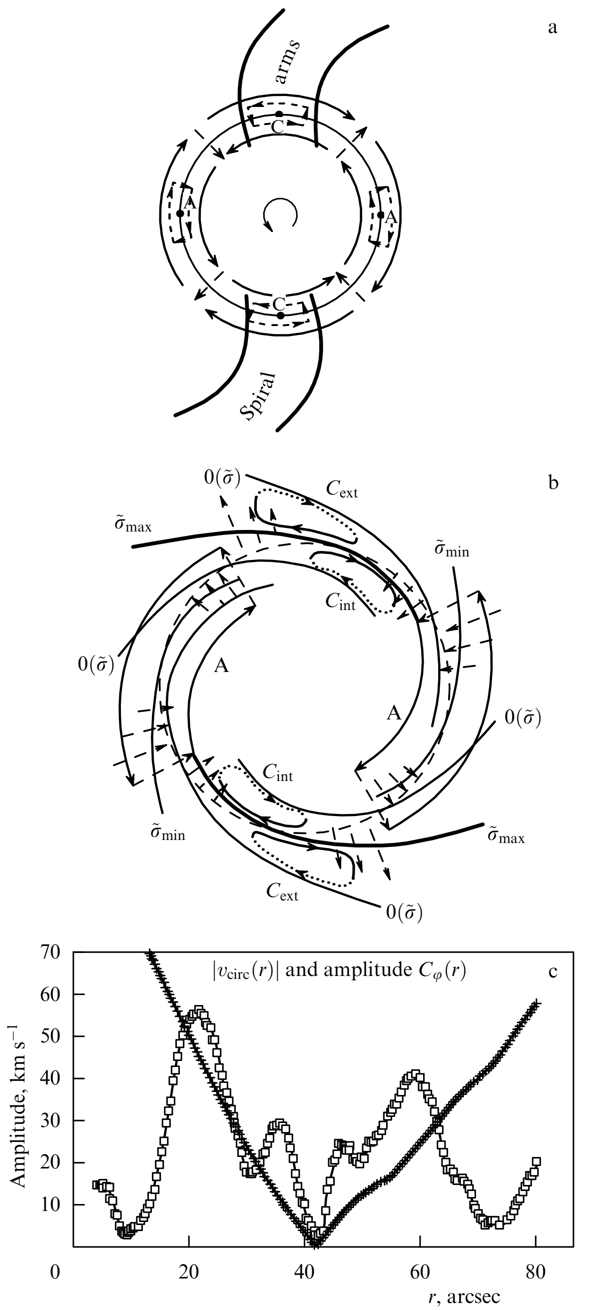

Figure 17. (a) The scheme of stationary (solid lines with arrows) and perturbed (dashed lines with arrows) velocity fields near the corotation circle in the frame corotating with a spiral pattern. (b) The velocity field in the frame corotating with a spiral pattern in the galaxy plane with a strong density wave: in addition to anticyclones located between spiral arms, there are two pairs of cyclones with centers on both sides of the corotation circle (the dashed circle) and from the line of the surface density maximum (the solid curve). (c) The perturbed azimuthal velocity amplitude C_φ (squares) calculated as a function of the radius and superimposed on the rotation velocity profile $|v_{\text{circ}}| = |v_{\text{rot}} - \Omega_{\text{ph}} r_{\text{c}}|$ (crosses) in the frame comoving with the spirals, $r_{\text{c}} \sim 42''$.

arrows in Fig. 17a). For the two-arm galaxy in Fig. 17a, perturbed velocities (dashed lines with arrows) change sign four times as the azimuthal angle changes by 2π. The perturbed velocities themselves form four vortex-like structures: two cyclones and two anticyclones (Fig. 17a). But because the directions of perturbed azimuthal velocities (in the density wave) coincide with the direction of rotation between spiral arms and are opposite on the spiral arms, the unperturbed rotation maintains anticyclone vortices and suppresses cyclones. Therefore, anticyclone vortices are always generated between the arms. Cyclones can be formed on spiral arms only if the perturbed velocities dominate; the rotation only suppresses them. Therefore, the perturbed velocity gradient dominating the rotation speed gradient in the spiral pattern reference frame turns out to be the condition for cyclone vortices to exist in the full velocity field of a galaxy:

$$\left|\frac{\partial \tilde{v}_\varphi}{\partial r}\right| > \left|\frac{\mathrm{d}v_{\text{circ}}}{\mathrm{d}r}\right| \equiv \left|\frac{\mathrm{d}\,(v_{\text{rot}} - \Omega_{\text{ph}} r_{\text{c}})}{\mathrm{d}r}\right| . \qquad (30)$$

We note that in a spiral galaxy, in the center-of-galaxy reference frame, perturbed velocities are always smaller than the rotation velocity, and in most cases are even much smaller $\left(|\tilde{v}_\varphi| \ll v_{\text{rot}}\right)$. But the perturbed velocity gradient can exceed the rotation velocity gradient in some regions of the disk due to the difference in the characteristic scales by which these values change. The presence of such regions at the corotation circle means that cyclones can appear in the velocity field of that galaxy. The ideas outlined above have led to the prediction of the existence of cyclones in galaxies with a pronounced spiral structure [39].

It can be shown that four variants of the cyclone vortex locations are possible. Three of them consist in forming pairs of cyclones whose centers lie on the corotation circle, inside or outside it. The fourth variant is a combination of the second and third ones: four cyclone vortices are formed on both sides of the corotation circle. The cyclones are slightly shifted with respect to the line of the surface density maxima (Fig. 17b) [41].

The theoretical prediction of the existence of cyclone vortices in the velocity fields of galaxies with pronounced spiral structures [39] was confirmed after the velocity field in the disk plane of galaxy NGC 3631 was reconstructed [33, 41]. (The apparent contradiction that the paper with the prediction was published later than the paper reporting the discovery was due to the anomalously long refereeing of the former).

In Fig. 17c, we compare radial dependences of the perturbed azimuthal velocity $|\tilde{v}_\varphi|$ and the disk rotation velocity of NGC 3631 in the comoving reference frame v_{circ}. The corotation radius in this galaxy is about $42''$. As can be seen from Fig. 17c, condition (30) is satisfied on both sides of the corotation circle (the slope of the curve for $\tilde{v}_\varphi$ is larger than for v_{circ}). Consequently, according to the prediction, we can expect the discovery of cyclones on both sides of the corotation circle as shown in Fig. 17b.

The reconstructed gas velocity field in the disk of NGC 3631 in the frame corotating with the spiral pattern is shown in Fig. 18a. We here see the structure of the velocity field, including two anticyclones between the spiral arms and four cyclones located exactly where the theory predicts (Fig. 17b) [33, 41].

8. Are there slow bars in spiral galaxies?

The well-known classical theory of rotating fluid bodies suggests that a rotating gravitating incompressible-fluid spherical body first transforms into a two-axial ellipsoid, and for faster rotation it transforms into a three-axial ellipsoid [42]. It can be concluded from this that the shape of a rotating fluid body is determined by its angular momentum.

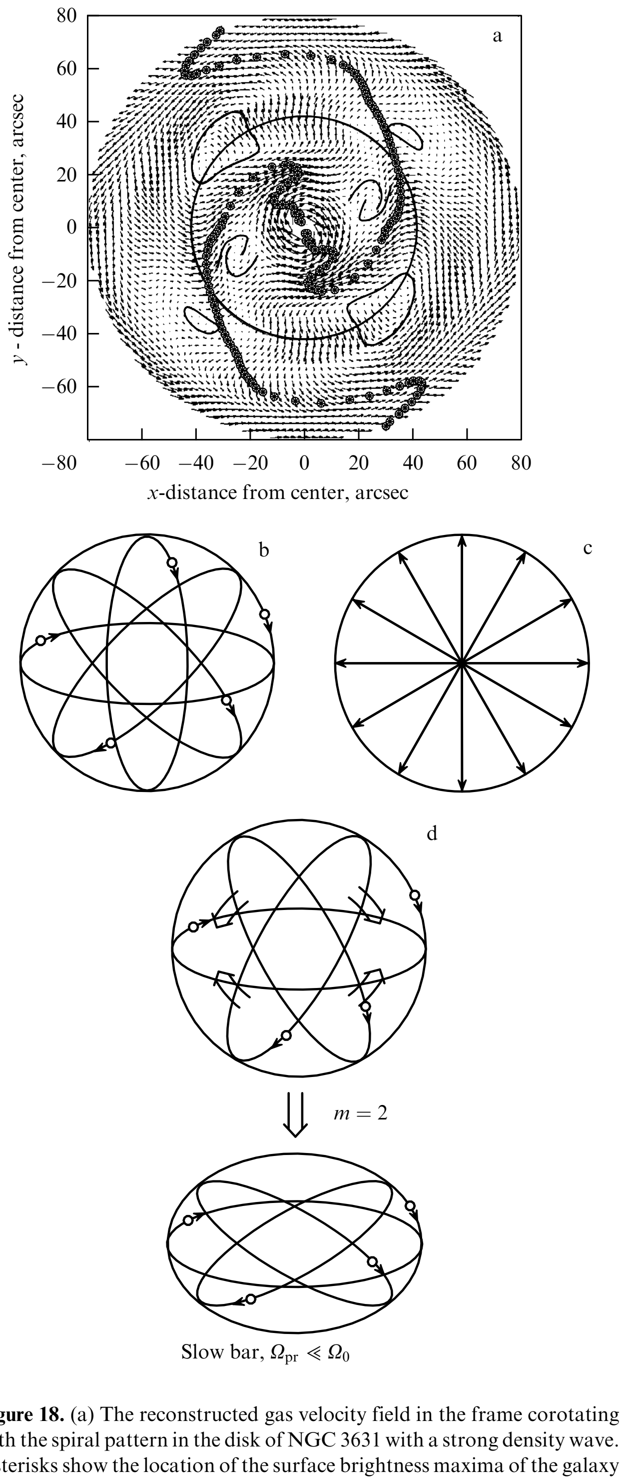

Figure 18. (a) The reconstructed gas velocity field in the frame corotating with the spiral pattern in the disk of NGC 3631 with a strong density wave. Asterisks show the location of the surface brightness maxima of the galaxy in the R-band (Fig. 15a); the location of cyclone vortices discovered in this galaxy is consistent with predictions of the density wave theory (Fig. 17b). (b, c) The Einstein model of a spherically symmetric stellar cluster: (b) — all particles move along circular orbits around the barycenter in the direction shown by the arrows; (c) — in the plane tangential to the arbitrary sphere at any point, the sum of the velocities of all particles is zero. (d) The scheme of transformation of a spherical collisionless system into an ellipsoidal one due to the instability of radial orbits.

Collisionless star systems do not have such a property. This means that on the one hand, we can find a spherical system with nonzero angular momentum, and on the other hand, there should be virtually irrotational ellipsoids in which the ratio of the rotational energy to gravitational (potential) energy is a small parameter. For elliptical galaxies, this ratio is about 13%. The form of elliptical galaxies is mainly determined by the anisotropy of their ‘temperatures’ (the ratio of velocity dispersions along and normal to the rotation axis is smaller than one). As regards the possibility of rotation of a spherically symmetric system, Lynden-Bell [43] showed that it is possible in principle.

This can be easily perceived when taking into account that starting from an irrotational spherical star system with a distribution function $f_0 = f_0(E, L)$, where E and L are the energy and angular momentum of a star, it is always possible to obtain an infinite set of distribution functions describing rotating spherical systems:

$$F_0(E, L, L_z) = \mu f_0(E, L)\,\Theta(L_z) + (1-\mu)\,f_0(E, L)\,\Theta(-L_z)\,, \qquad (31)$$

where μ is a parameter, $0 \leqslant \mu \leqslant 1$, and $\Theta(L_z)$ is the step function. The transformation described by Eqn (31) means that we transform velocities of some group of stars such that the number of particles with $L_z > 0$ becomes μ, and the number of particles with $L_z < 0$ becomes $1-\mu$, $\mu \neq 1/2$. It is easy to see that neither the system density $\rho_0(r)$ nor its gravitational potential $\Phi_0(r)$ are then modified.

As an example, we consider a system of particles (stars) in circular orbits (Fig. 18b, c). The distribution function [44]

$$f_0 = \frac{\rho_0(r)}{2\pi v_0(r)}\,\delta(v_r)\big[v_\perp - v_0(r)\big]\,,$$
$$v_\perp^2 \equiv v_\theta^2 + v_\varphi^2\,, \quad v_0^2(r) = r\Phi_0'(r)\,, \qquad (32)$$

(where $\Phi(r)$ is the gravitation potential) describes the situation where the sum of all particle velocities vanishes in the plane tangential to any sphere at any point, i.e., the system does not rotate as a whole.

For convenience, we choose some direction (the z axis) and, in the equatorial plane, create an excess of particles rotating in one direction around the axis over those rotating in the opposite direction. Such a system has a nonzero total angular momentum.

In the stationary and axially symmetric case $\partial/\partial t = \partial/\partial\varphi = 0$ and $\Phi_0 = \Phi_0(r)$, we have the kinetic equation [35, 44]

$$\frac{v_\perp}{r}\left(\cos\alpha\,\frac{\partial f_0}{\partial\theta} - \sin\alpha\cos\theta\,\frac{\partial f_0}{\partial\alpha}\right) + v_r\left(\frac{\partial f_0}{\partial r} - \frac{v_\perp}{r}\,\frac{\partial f_0}{\partial v_\perp}\right) + \left(\frac{v_\perp^2}{r} - \frac{\mathrm{d}\Phi_0}{\mathrm{d}r}\right)\frac{\partial f_0}{\partial v_r} = 0\,. \qquad (33)$$

It can be observed that Eqn (33) is satisfied, for example, for the function of the form [45, 46]

$$f_{0\mu} = \frac{\rho_0}{2\pi v_0}\,\delta(v_r)\,\delta(v_r - v_0)(1 + \mu\sin\theta\sin\alpha)\,, \quad |\mu| \leqslant 1\,. \qquad (34)$$

We can now calculate the angular rotation velocity of a homogeneous ($\rho_0 = \mathrm{const}$) sphere [45, 46]. By definition, the linear rotation velocity at the point $\mathbf{r}$ is

$$\big\langle v_\varphi(\mathbf{r})\big\rangle = \frac{1}{\rho_0}\int v_\varphi F_{0\mu}\,\mathrm{d}\alpha\,v_\perp \mathrm{d}v_\perp\,\mathrm{d}v_r = \frac{1}{2}\,\mu\,\Omega_0 r\sin\theta\,, \qquad (35)$$

where we use the formula $v_\varphi = v_\perp\sin\alpha$. The expression for $\big\langle v_\varphi(\mathbf{r})\big\rangle$ implies that the angular rotation velocity of the system $\Omega_{\rm rot}$ is directly related to the parameter μ:

$$\Omega_{\rm rot} = \frac{\mu \Omega_0}{2}\,, \qquad (36)$$

where Ω_0 is the rotation velocity of particles in circular orbits. This result suggests that the homogeneous sphere rotates as a solid body.

How can one qualitatively imagine the formation of bars in galaxies? According to observations, galaxies show a broad specific angular momentum distribution. Protogalaxies that acquired comparatively large angular momentum formed massive disks, where the so-called bar instability leads to the formation of a large 'fast' bar. The ends of the bar, where trailing spiral arms originate, rotate with the linear velocity coincident with that of the differentially rotating disk (if the bar is rigidly connected with spirals). In this region of the disk near the bar ends, the main (corotation) resonance of the galaxy disk is located. Such a bar is called fast, in contrast to a slow bar whose ends rotate with a velocity much smaller than that in the adjacent region.

Slow bars could form in protogalaxies with lower angular momenta than in galaxies with fast bars. The formation of a slow bar could be the result of the instability of radial orbits. The central density increase that forms during the radial collapse and hence consists of radially elongated orbits of stars turns out to be 'colder' in the transverse direction than in the radial one. During the collapse, most gravitational energy is transformed into radial motion. It is therefore not surprising that the radial velocity dispersion is higher than the transverse one. Small transverse perturbations begin growing, which cannot be precluded by the small transversal velocity dispersion (Fig. 18d). In fact, an anisotropic Jeans instability develops in the transverse direction and increases the velocity dispersion in this direction and correspondingly decreases the 'eccentricity' of stellar orbits (the orbits are not closed in general).

Such an instability of radial (or elongated) orbits was predicted by Zeldovich et al [47] in 1972. The instability of radial orbits belongs to the class of Jeans instabilities. This means that when such an instability develops, the amplitude of the largest collective oscillation mode transforming the system into a two-axial ellipsoid grows most rapidly (Fig. 18d) [48]. The ellipsoid rotates slowly with a precession frequency much smaller than the characteristic rotation frequency of stars ($\Omega_{\rm pr} \ll \Omega_0$), hence the name 'slow bar.' The necessary condition for the radial orbit instability $\mathrm{d}\Omega_{\rm pr}/\mathrm{d}L > 0$, where L is the angular momentum of a star, exactly coincides with the slow bar formation condition due to capture of stars by the gravitational bar potential [49].

According to Polyachenko, the location of the slow bar must have the following properties:

(1) its radius is limited by the inner – inner Lindblad resonance;

(2) in the case of a slow bar, the main spiral arms of a galaxy, being trailing spirals, are bounded from the central region by the outer – inner Lindblad resonance;

(3) the ends of the slow bar are connected to the principal spiral arms by leading spirals with the azimuthal size $\approx 180°$.

Figure 19a shows the response of a gaseous disk to the gravitational potential of a slow bar, first calculated in [50]. As we see, the response includes two spirals. The first represents a part of the trailing (external) spiral, which is the continuation of the principal trailing spiral arms of the galaxy. The second spiral turns out to be leading. Occupying

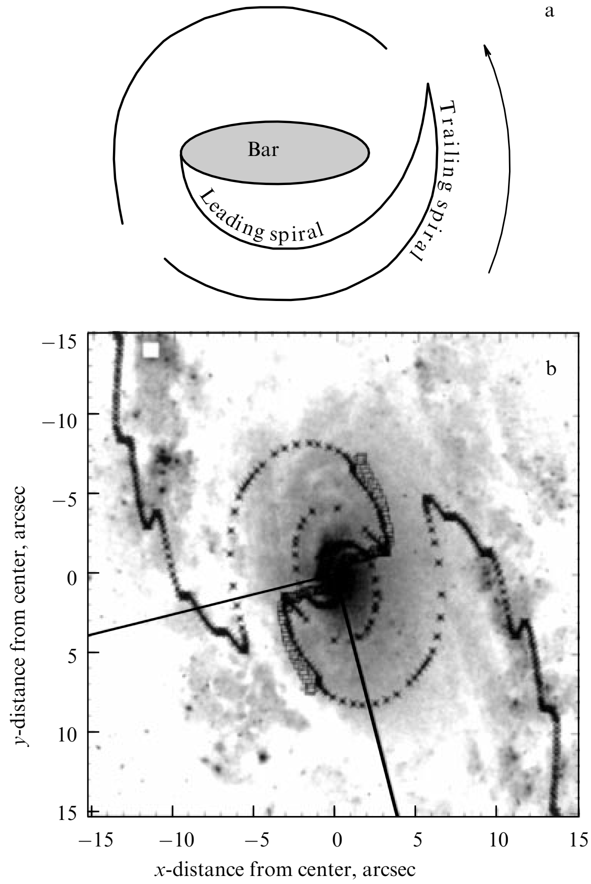

Figure 19. (a) The response of a gaseous disk to the gravitational potential of a slow bar [50]. (b) Locations of the second Fourier harmonic maximum in the broadband optical image ($\times$) and the near-IR band H ($\square$), superimposed on the optical image of the central part of NGC 157 [51]. The galaxy rotates counter-clockwise; this means that the leading spiral originates near the ends of the bar, makes half a turn, and transforms into the external trailing spiral, which forms the grand design of this galaxy. Qualitative agreement of the bar – spiral structures is clearly seen in panels (a) and (b).

a narrow radial part of the disk, it is very tightly wound and makes half a turn between the bar and the external spiral. The leading spiral is localized between the inner – inner (IILR) (ends of the bar) and the outer – inner (OILR) (beginning of the trailing spiral) Lindblad resonances.

Exactly this form of spiral arms in the vicinity of the inner Lindblad resonance was discovered by us [51] based on the analysis of photometric data of the galaxy NGC 157 obtained by the Hubble Space Telescope (the data are available from the HST archive). Figure 19b shows the location of the maximum of the second harmonic of the surface brightness map of the central region of NGC 157 in the visible range (mean wavelength ≈ 5852 Å, band width ≈ 1873 Å) as a function of radius. The $10''$ bar is clearly seen when the second harmonic of the near-infrared (IR H-band) surface brightness map is superimposed on the figure. The IILR exactly occurs at the $5''$ radius, the OILR is at $8''$, and the leading spirals connect the ends of the bar located at $5''$ to the beginning of the trailing spiral (located at $10''$) within $2''$ of the OILR.

Thus, these results were found to be in very good agreement with theoretical predictions, which is a serious argument in favor of the existence of a slow bar in NGC 157.

9. The observed envelope soliton-like oscillatory structure in the spiral arm of NGC 1365

Most of the mass of the interstellar gas in galaxies is in the form of neutral hydrogen, and therefore observations on the HI 21 cm line are the most direct means of measurement of the gaseous disk velocity field. But the present-day angular resolution of radio observations that can be reached over a large field is significantly lower than that of optical observations. This is why almost all velocity fields of spiral galaxies (except the closest ones) studied in detail have been obtained from line-of-sight velocity measurements on the Hα line.

Radio observations of the galaxy NGC 1365 are special. This giant nearby galaxy has a well-defined spiral structure, and hence the resolution on the 21 cm line is sufficient to study the inner detailed structure of spiral arms in the galaxy gaseous disk.

Observations demonstrate that neutral hydrogen (HI) is concentrated in spiral arms. With the volume adiabatic index $\gamma = 5/3$, the atomic gas density at the front of a 'classical' strong shock wave can attain a value four times as high as before the front because the maximum density ratio is $(\gamma + 1)/(\gamma - 1)$. But observations show that this ratio can be almost an order of magnitude higher. The additional compression of gas compared to that expected in the 'classical' shock is due to the strong radiative cooling of gas (free – free transitions). However, we are now interested in structures on a scale much larger than the shock front width of the spiral density wave in an atomic gas.

The question as to the structures of spiral arms in an atomic gas is tightly related to another issue, which has a quarter-century history, that gas disks of galaxies (by their main parameters) are at the dynamical instability boundary. This appears natural: as the instability develops, the velocity dispersion increases and the disk 'heats up' and becomes more and more stable until the actual reason for heating disappears and the disk approaches the stability boundary. The analysis in [52], as well as later ones, confirmed this assumption using different samples of spiral galaxies.

Mikhailovsky, Petviashvili, and Fridman [31, 32] showed that the nonlinear dynamics of a gaseous galactic disk at the gravitational instability boundary is described by the nonlinear Schrödinger equation. This allowed them to hypothesize that spiral arms in galaxies are envelope solitons; these solitons can be described by one of the solutions of the nonlinear Schrödinger equation (Fig. 20a). The concept that spiral arms that keep their form in a differentially rotating galaxy disk are solitons endowed with the property of being stable when propagating in inhomogeneous streams and media by definition appears quite natural and appealing.

In Fig. 20b, we can see that real spiral arms in the gaseous disk of the galaxy NGC 1365 indeed demonstrate an

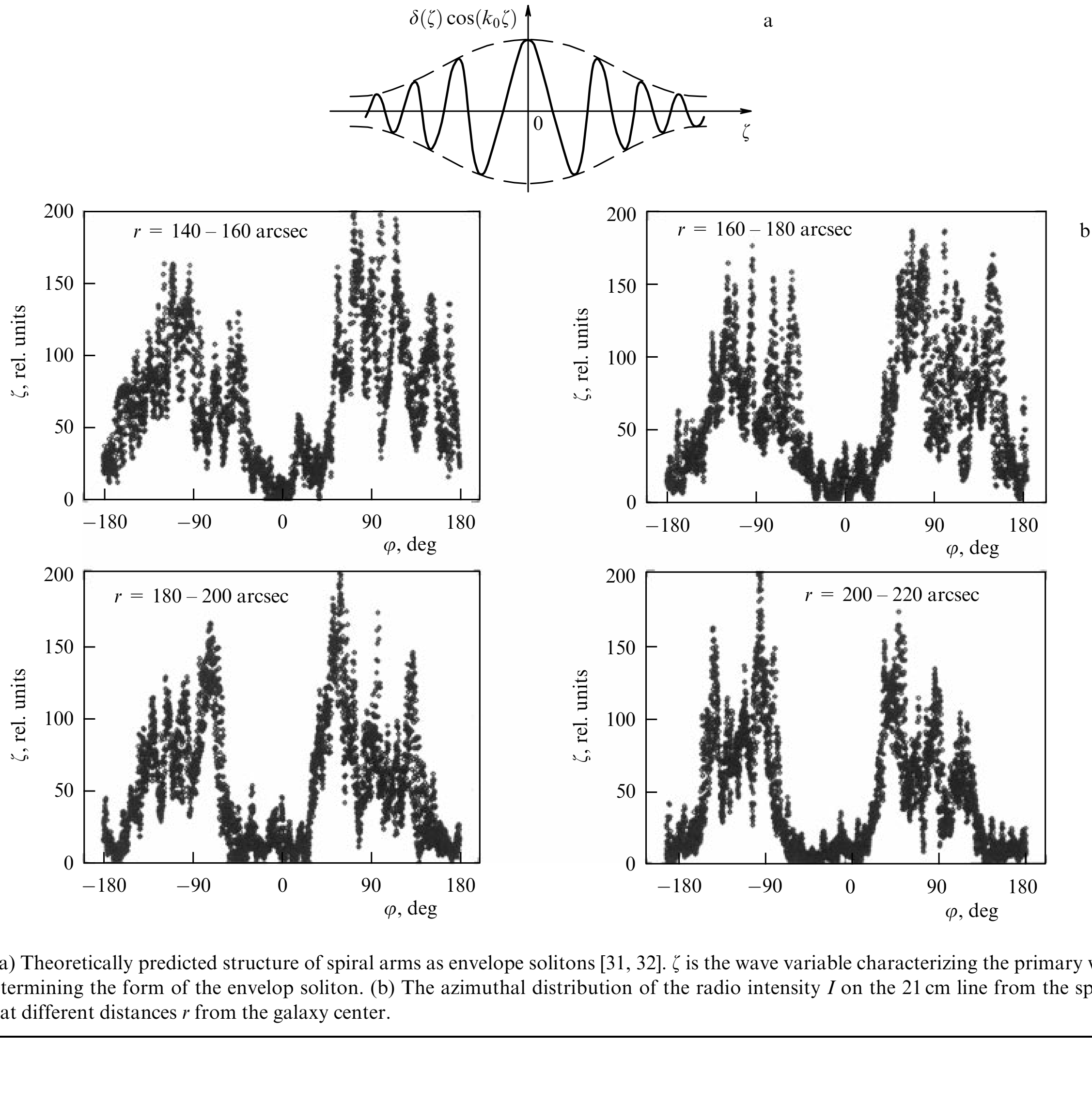

Figure 20. (a) Theoretically predicted structure of spiral arms as envelope solitons [31, 32]. ζ is the wave variable characterizing the primary wave, δ is a function determining the form of the envelop soliton. (b) The azimuthal distribution of the radio intensity I on the 21 cm line from the spiral galaxy NGC 1365 at different distances r from the galaxy center.

oscillatory structure — the large-scale envelope curve describes two spiral arms, each filled with small-scale quasi-periodic density variations. Such a structure is well consistent with being an envelope soliton predicted by the theory (Fig. 20a).

We note that the secondary gravitational instability generating shorter-wavelength secondary perturbations in a gas 'compressed' by the primary instability could have similar observational manifestations.

10. Conclusion

The main results considered in this review can be summarized as follows.

• Using the setup designed at the Kurchatov Institute for modeling the centrifugal instability in gaseous disks of galaxies with a rotation velocity jump, we discovered anticyclone vortices whose centers were located between spiral arms near the velocity jump. This served as a basis for predicting such structures in real grand-design galaxies with rotation velocity jumps.

• In the gaseous disk of the spiral galaxy Mrk 1040 with a large rotation velocity jump, we discovered anticyclones located exactly as predicted by the rotating shallow water experiments: the anticyclone centers were found between spiral arms near the rotation velocity jump.

• In the solar vicinity of the gaseous disk of our Galaxy in the region of decreasing rotation velocity, we have found anticyclones with the size ≈ 4 kpc. Their origin can be naturally related to the spiral structure of our Galaxy, considering the solar galactocentric orbit location near the corotation circle.

• The theory predicts the simultaneous emerging of spiral arms and vortices in the spiral density wave irrespective of the excitation mechanism: a hydrodynamic instability when the rotation velocity jump is present or a gravitational instability when no drastic gradients of the disk parameters are observed. According to theoretical predictions, giant anticyclones were discovered in grand-design galaxies with smooth rotation curves: NGC 157, NGC 3631, NGC 1365, and NGC 6148. In all cases, anticyclones are located between spiral arms near the corotation circle, i.e., exactly where the theory predicts.

• In galaxies with a large-amplitude spiral density wave, the theory predicts the existence of both anticyclones and cyclones, with the centers of the latter located at the surface density maxima on spiral arms and near the corotation circles, or on opposite sides from the corotation circle and the line of the density maxima of spiral arms. Giant cyclones were discovered in the large-amplitude grand-design spiral galaxy NGC 3631. The localization of these cyclones is fully consistent with theoretical predictions.

• A slow bar was discovered in the spiral galaxy NGC 157. This closed the discussion of more than a quarter-century on the possible existence of slow bars in galaxies. In this galaxy, a tightly wound leading spiral, which makes a half-turn in a narrow radial region of the disk between inner – inner and outer – inner Lindblad resonances, is found between the ends of the bar and the main system of trailing spiral arms. Exactly such a nontrivial structure was predicted earlier to be the form of response of the galaxy disk to the potential of a slow (and only slow) bar, which definitely proves its existence in the center of NGC 157.

• The inner oscillatory structure of spiral arms in the gaseous disk of NGC 1365, recently discovered in a neutral hydrogen distribution obtained from observations on the 21 cm line, shows an envelope-soliton form. The concept of spiral density waves as envelope solitons was put forward in papers coauthored by the present author about 25 years ago.

• The discovery of predicted galaxy structures required the observational base to be significantly developed and new methods of data processing to be elaborated.

• The method of restoring the full vector velocity field of gaseous disks in grand-design galaxies from the observed one-component line-of-sight velocity field is elaborated, aimed at solving an ill-posed problem, and it is therefore principally important that it includes several independent observational tests to verify the correctness of the model assumptions used.

• An observational test is elaborated to check the wave nature of the spiral structure observed in spiral galaxies.

• An observational test is elaborated to check the nature of vertical motions in disk galaxies, which can be used to clarify whether they are due to bending oscillations or the z-component of the density wave velocity field.

All results are new and have no foreign analogs.

References

1. Afanas'ev V L et al. *Astrofiz.* **28** 243; **29** 155 (1988) [*Astrophys.* **28** 142 **29** 497 (1988)]; *Astron. Zh.* **68** 1134 (1991); **69** 19 (1992) [*Sov. Astron.* **35** 569 (1991); **36** 10 (1992)]
2. Baev P V, Makov Yu N, Fridman A M *Pis'ma Astron. Zh.* **13** 964 (1987) [*Sov. Astron. Lett.* **13** 406 (1987)]; Baev P V, Fridman A M *Astron. Tsirk.* (1535) 1 (1989)
3. Fridman A M *Usp. Fiz. Nauk* **125** 352 (1978) [*Sov. Phys. Usp.* **21** 536 (1978)]
4. Lindblad È *Stockholms Observat. Ann.* **29** 155 (1941); Lin C C, Shu F H *Astrophys. J.* **140** 646 (1964); *Proc. Natl. Acad. Sci. USA* **55** 229 (1966)
5. Landau L D, Lifshitz E M *Gidrodinamika* (Fluid Mechanics) (Moscow: Nauka, 1988) § 108 [Translated into English (Oxford: Pergamon Press, 1987)]
6. Fridman A M *Zh. Eksp. Theor. Fiz.* **98** 1121 (1990) [*Sov. Phys. JETP* **71** 627 (1990)]
7. Fridman A M "Theory of gradient instabilities of a gaseous Galactic disc and rotating shallow water", in *Dynamics of Astrophysical Discs* (Ed. J A Sellwood) (Cambridge: Cambridge Univ. Press, 1989) p. 185
8. Morozov A G et al. *Pis'ma Zh. Eksp. Theor. Fiz.* **39** 504 (1984) [*JETP Lett.* **39** 613 (1984)]; *Usp. Fiz. Nauk* **145** 161 (1985) [*Sov. Phys. Usp.* **28** 101 (1985)]; Fridman A M et al. *Phys. Lett. A* **109** 228 (1985)
9. Nezlin M V et al. *Pis'ma Astron. Zh.* **12** 504 (1986) [*Sov. Astron. Lett.* **12** 213 (1986)]
10. Jeans J H *Astronomy and Cosmogony* 2nd ed. (Cambridge: The Univ. Press, 1929)
11. Fridman A M et al. *Astrophys. Space Sci.* **252** 115 (1997)
12. Lyakhovich V V et al. *Astron. Zh.* **74** 509 (1997) [*Astron. Rep.* **41** 447 (1997)]
13. Morozov A G *Astron. Zh.* **56** 498 (1979) [*Sov. Astron.* **23** 278 (1979)]
14. Combes F *Annu. Rev. Astron. Astrophys.* **29** 195 (1991)
15. Sumin A A, Fridman A M, Haud U A *Pis'ma Astron. Zh.* **17** 698, 779 (1991) [*Sov. Astron. Lett.* **17** 295, 329 (1991)]
16. Gor'kavyi N N, Fridman A M *Fizika Planetnykh Kolets*: Nebesnaya Mekhanika Sploshnoi Sredy (Physics of Planetary Rings: Celestial Mechanics of Fluids) (Moscow: Nauka, 1994) [Translated into English: Fridman A, Gor'kavyi N *Physics of Planetary Rings*: *Celestial Mechanics of Continuous Media* (New York: Springer, 1999)]
17. Landau L D *Dokl. Akad. Nauk SSSR* **44** 151 (1944)
18. Loitsyanskiy L G *Mekhanika Zhidkosti i Gaza* (Mechanics of Liquids and Gases) 4th ed. (Moscow: Nauka, 1973) [Translated into English (New York: Begell House, 1995)]

19. Fridman A M *Usp. Fiz. Nauk* **160** 179 (1990) [*Sov. Phys. Usp.* **33** 865 (1990)]
20. Nezlin M V, Snezhkin E N *Vikhri i Spiral'nye Struktury*: Astrofizika i fizika Plazmy v Opytakh na Melkoi Vode (Vortices and Spiral Structures: Astrophysics and Plasma Physics in Shallow Water Experiments) (Moscow: Nauka, 1990); *Rossby Vortices Spiral Struktures, Solitons*: *Astrophysics and Plasma Physics in Shallow Water Experiments* (Berlin: Springer-Verlag, 1993)
21. Pasha I I *Pis'ma Astron. Zh.* **11** 3 (1985) [*Sov. Astron. Lett.* **11** 1 (1985)]
22. Afanas'ev V L, Fridman A M *Pis'ma Astron. Zh.* **19** 787 (1993) [*Astron. Lett.* **19** 319 (1993)]
23. Efremov Yu N *Pis'ma Astron. Zh.* **9** 94 (1983) [*Sov. Astron. Lett.* **9** 51 (1983)]
24. Avedisova V S *Astrofizika* **30** 140 (1989) [*Astrophys.* **30** 83 (1989)]
25. Mishurov Yu N et al. *Astron. Astrophys.* **323** 775 (1997)
26. Fridman A M "Dynamics of disks in the Milky Way: some solved problems and some puzzles", in *Physics of the Gaseous and Stellar Disks of the Galaxy* (Astron. Soc. of the Pacific Conf. Ser., Vol. 66, Ed. I R King) (San Francisco: Astron. Soc. of the Pacific, 1994) p. 15
27. Fridman A M et al., in *Unsolved Problems of the Milky Way*: *Proc. of the 169th Symp. of the Intern. Union, The Hague, The Netherlands, August 23 – 29, 1994* (Eds L Blitz, P Teuben) (Dordrecht: Kluwer Acad. Publ., 1996) p. 597
28. Lyakhovich V V, Fridman A M, Khoruzhii O V *Astron. Zh.* **73** 24 (1996) [*Astron. Rep.* **40** 18 (1996)]
29. Lyakhovich V V, Fridman A M, Khoruzhii O V, in *Neustoichivye Protsessy vo Vselennoi* (Unstable Processes in the Universe) (Ed. A G Masevich) (Moscow: Kosmosinform, 1994) p. 194
30. Contopoulos G *Astron. Astrophys.* **64** 323 (1978)
31. Mikhailovskii A B, Petviashvili V I, Fridman A M *Pis'ma Zh. Eksp. Theor. Fiz.* **26** 129 (1977) [*JETP Lett.* **26** 121 (1977)]
32. Mikhailovskii A B, Petviashvili V I, Fridman A M *Astron. Zh.* **56** 279 (1979) [*Sov. Astron.* **23** 153 (1979)]
33. Fridman A M et al. "Gas motions in the plan of the spiral galaxy NGC 3631" *Mon. Not. R. Astron. Soc.* **323** 651 (2001)
34. Fridman A M et al. *Pis'ma Astron. Zh.* **24** 883 (1998) [*Astron. Lett.* **24** 764 (1998)]
35. Fridman A M, Polyachenko V L *Physics of Gravitating Systems* Vols 1, 2 (New York: Springer-Verlag, 1984)
36. Knapen J H "Atomic hydrogen in the spiral galaxy NGC 3631" *Mon. Not. R. Astron. Soc.* **286** 403 (1997)
37. Fridman A M et al. "Investigation of the dynamics of spiral galaxies on the base of 3D vector velocity field of their gaseous disks reconstructed from observed line-of-sight velocity field", in *The Combination of Theory, Observations, and Simulation for the Dynamics of Stars and Star Clusters in the Galaxy, 23rd Meeting of the IAU, Joint Discussion 15, 25 August 1997, Kyoto, Japan, Meeting Abstracts* (Ed. J Andersen) (Dordrecht: Kluwer Acad. Publ., 1998) p. 39
38. Fridman A M et al. "Discovery of new structures – giant antycyclones – in disks of spiral galaxies", in *Searching for Absolute Values and Unity in the Sciences*: *Science for the Benefit of Humanity*: *Commemorative Volume of the Twenty-first Intern. Conf. on the Unit of the Sciences, 1997* (Lexington, Ky.: ICCU, 1997)
39. Fridman A M et al. *Astron. Astrophys.* **371** 538 (2001)
40. Fridman A M et al. "New structures in galactic disks: predictions and discoveries", in *Galaxy Disks and Disk Galaxies* (Astron. Soc. of the Pacific Conf. Ser., Vol. 230, Eds J G Funes, E M Corsini) (San Francisco, Calif.: Astron. Soc. of the Pacific, 2001) p. 187
41. Fridman A M et al. *Phys. Lett. A* **264** 85 (1999)
42. Chandrasekhar S *Ellipsoidal Figures of Equilibrium* (New Haven: Yale Univ. Press, 1969)
43. Lynden-Bell D "Can spherical clusters rotate?" *Mon. Not. R. Astron. Soc.* **120** 204 (1960)
44. Mikhailovskii A B, Fridman A M, Epelbaum Ya G *Zh. Eksp. Theor. Fiz.* **59** 1608 (1970) [*Sov. Phys. JETP* **32** 878 (1971)]
45. Synakh V S, Fridman A M, Shukhman I G *Dokl. Akad. Nauk SSSR* **201** 827 (1971) [*Sov. Phys. Dokl.* **16** 1062 (1972)]
46. Fridman A M, Shukhman I G *Dokl. Akad. Nauk SSSR* **202** 67 (1972) [Sov. Phys. Dokl. **17** 44 (1972)]
47. Zel'dovich Ya B et al., Preprint No. 7-72 (Irkutsk: Institute of Terrestrial Magnetism, Ionosphere and Radio Wave of the Siberian Branch of the Academy of Sciences of the USSR, 1972)
48. Polyachenko V L *Pis'ma Astron. Zh.* **7** (3) 142 (1981) [*Sov. Astron. Lett.* **7** (3) 79 (1981)]
49. Lynden-Bell D *Mon. Not. R. Astron. Soc.* **187** 101 (1979)
50. Polyachenko V L, in *Physics of the Gaseous and Stellar Disks of the Galaxy* (Astron. Soc. of the Pacific Conf. Ser., Vol. 66, Ed. I R King) (San Francisco, Calif.: Astron. Soc. of the Pacific, 1994) p. 103
51. Fridman A M , Khoruzhii O V *Phys. Lett. A* **276** 199 (2000)
52. Zasov A V, Simakov S G *Astrofizika* **29** 190 (1988) [*Astrophys.* **29** 518 (1988)]